Drag Reduction in Turbulent Flow Using Biopolymers

A Thesis
Submitted in partial fulfillment of
requirements for the degree of

Master of Engineering
in
Thermal Engineering

by

B. Satya Prashant

Registration No.: 801583006

Under the Supervision of

Mr. Sumeet Sharma
(Associate Professor, MED)

Dr. D. Gangacharyulu
(Professor, CHED)

DEPARTMENT OF MECHANICAL ENGINEERING
THAPAR UNIVERSITY, PATIALA

June, 2017

Certificate

This is to certify that the thesis entitled "**Drag Reduction in Turbulent Flow Using Biopolymers**" is an authentic record of work carried out by B. Satya Prashant as requirement for the award of the degree of **Master of Engineering** in **Thermal Engineering** at **Thapar University, Patiala,** during July, 2015 to July, 2017. No part of the matter embodied in this report has been submitted to any other university or institute for the award of any degree.

(Sumeet Sharma)
Mechanical Engineering Department
Thapar University, Patiala – 147004

(D. Gangacharyulu)
Chemical Engineering Department
Thapar University, Patiala - 147004

Declaration

I, **B. Satya Prashant,** hereby declare that the thesis, entitled **"Drag Reduction in Turbulent Flow Using Biopolymers"**, submitted to the **Thapar University,** in partial fulfillment of the requirements for the award of the **Master of Engineering** in **Thermal Engineering** submitted in Mechanical Engineering Department, Thapar University is a record of original and independent research work done by me during the period 2015–2017, under the supervision and guidance of Mr. Sumeet Sharma, Associate Professor, Mechanical Engineering Department and Dr. D. Gangacharyulu, Professor, Department of Chemical Engineering, Thapar University. The work contained in this thesis has not been previously submitted to meet the requirements for a degree or diploma at this or any other higher education institution.

B. Satya Prashant

(B. Satya Prashant)
Regd. No 801583006

Dedicated to

My parents

Acknowledgements

I would like to express my deep sense of gratitude to Mr. Sumeet Sharma and Dr. D. Gangacharyulu for their invaluable suggestions, excellent supervision, constant encouragement, thought provoking discussions and unabashed inspiration in nurturing the work and during the preparation of manuscript throughout the research work.

I offer my special regard to Mr. Kamaljit Singh, Research Scholar, Department of Chemical Engineering, Thapar University, Patiala, India, for providing immense support in performing the experimental work throughout my research work.

I also express my indebtedness to my family for their infinite support at each and every part of my life.

(B. Satya Prashant)

Abstract

The aim of this study is to investigate experimentally the effect of bio-polymers in the process of drag reduction in a single phase water flow at high Reynolds number. By using biopolymers, makes the entire process of polymer induced drag reduction economical and more versatile. A comparative study has been carried out using two high molecular weight bio-polymers guar gum

D and hydroxyethyl cellulose (HEC). These two additives of different concentrations and flow rates, taken as parameters of study to observe the influence in drag reduction. Different concentrations of 1000 ppm, 1500 ppm, 2000 ppm, 2500 ppm and 3000 ppm are used at high Reynolds numbers to find the percentage of maximum drag reduction (%MDR) in the turbulent flow inside the pipe. In this experimental study shear viscosity of each concentration is measured by Brookfield viscometer, and validated with power law. From this study, it is found that there is significant decrease in skin friction drag with increase in concentration of polymer solutions. The maximum percentage of drag reduction is about 77.5% (HEC) as compared to 75% (GG) at high Reynolds number of 44309, with 3000 ppm concentration. The results found, are further validated

with the universally accepted maximum drag reduction (MDR) asymptote or Virk's asymptote. The mechanical degradation of the polymers due to the centrifugal pump is also studied and found that hydroxyethyl cellulose (HEC) has better self-life stability than the guar gum (GG). The test section consists of horizontal pipe of 19 mm inner diameter and 1524 mm long. The master solution is prepared by paddle stirrer with the range of 1600-2500 rpm. Injection of master solution in the test section is done by peristaltic pump at a rate of 450cc/hr., and the pressure difference across the pipe in the test section is measured by U-tube manometer. The pH of each concentration of the polymer solutions is also measured. The pH of guar gum lies within the range of 4-7 and that for hydroxyethyl cellulose lies between 7 to 8.2.

Keywords**:** Drag reduction, Guar gum, Hydroxyethyl cellulose.

Table of Contents

List of Figures

List of Tables

Nomenclature

	Surface area, m^2
E	Diameter, m
V	Velocity, m/s
Coefficient of friction	
f	Frictional factor
g	Acceleration due to gravity, m/s^2
L	Length, m
r	Radius of the pipe, m
v	Volume, m^3
p	Pressure gradient, kPa
Δh	Change in mercury level from scale, m
Δx	Finite distance on the test section, m
Q	Discharge, m^3/s
h_L	Head loses, m
hp	Horse power, kW
h	Hydraulic pump power, kW
W^o	Onset wave number

Greek Symbols

δ	Slope increment
M	Viscosity, $N\text{-}s/m^2$
P	Density, kg/m^3
T	Wall shear stress, kPa

Subscripts

m	Mercury
w	Water
e	Onset of fully developed flow
h	Hydraulic power
l	Losses
wa	Wall

Acronyms

LPH	Liters per hour
LPM	Liters per minute
GG	Guar Gum
HEC	Hydroxyethyl Cellulose
DR	Drag reduction
DRP	Drag reducing polymers
Re	Reynolds number
MDR	Maximum drag reduction
cc/hr	Cubic centimeter per hour
Ppm	Parts per million

Chapter 1
Introduction

1.1 Introduction

Drag (fluid resistance) is the force acting opposite to the relative motion of fluid moving with respect to the surrounding surface. This may exist between two fluid layers or two surfaces or a fluid and a solid surface. It can also be defined as pressure head losses due to the friction between flow and the pipe surface which reduces the plug flow, this requires more energy for pumping the fluid [1]. Though the ultimate cause of drag is viscous friction, the turbulent drag is independent of viscosity. Drag force decreases the fluid velocity relative to the solid surface in the fluid's path. Drag force in the turbulent flow can be expressed by

$$= \frac{}{2} \cdot \cdot \qquad (1)$$

where V is velocity, ρ is fluid density, is coefficient of friction and is surface area.

Different types of drag forces are classified in Figure 1.1.

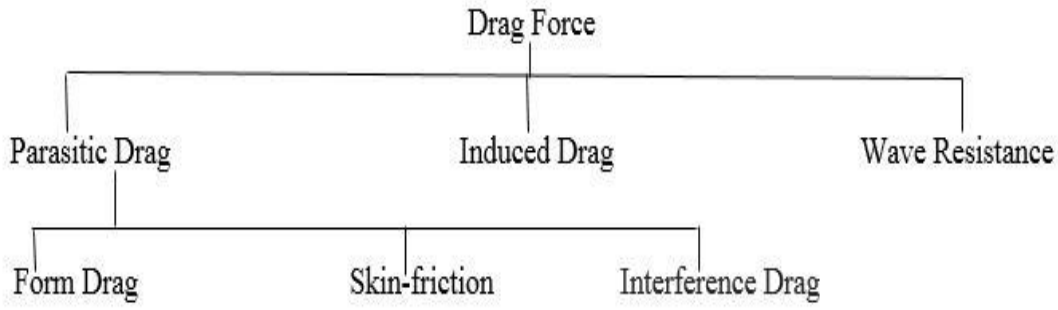

Figure 1.1: Classification of drag forces.

Parasitic drag: It is due to the combined effect of form drag, skin-friction drag and interference drag. Form drag or pressure drag is the force acted upon the body by flowing fluid due to decrease in pressure due to boundary layer separation. Skin-friction is due to the shear forces between the surface and the fluid, it is directly related to wetted surface area. Interference drag is due to the geometrical proximities.

Induced drag: This results from the generation of trailing vortex system downstream of a lifting surface, induced by the lift force.

Wave resistance: It is the form of drag that affects surface watercrafts and reflects the energy required to push water out of the way of the hull.

1.2 Types of Flows

The different flow regimes in a pipe describes the nature of the fluid flow, it is shown in Figure 1.2.

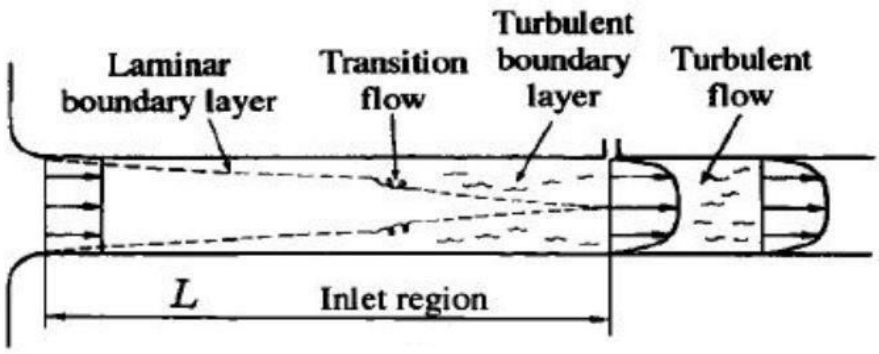

Figure 1.2: Different flow regimes in a pipe.

1. Laminar flow:

A stable well-defined state of flow in which the adjacent fluid particles move alongside one another forming laminaes. The flow is laminar when Reynolds number (Re) $\leq$ 2300

2. Transition flow:

An unstable flow at a Reynolds number greater than a critical value, but not sufficiently high that the flow has reached a fully developed turbulent flow state. The transitional flows often oscillate randomly between laminar and turbulent states. The flow is in transitional state when Reynolds number (Re) is in the range of $2300 \leq Re \leq 4000$.

3. Turbulent flow:

Turbulent flows are always at Reynolds numbers above the critical value. Turbulence is the breakdown of orderly laminar flow into a state of random fluctuations of velocity. The haphazard movement of fluid particles makes it impractical to predict the motion of the fluid particle with respect to space and time. In this surface shear stresses are much higher, and head

loss is greatly increased as compared to corresponding laminar flows. The flow is turbulent when Reynolds number (Re) ≥ 4000.

1.3 Drag Reducing Additives

Drag reducing agents can be classified under the following three categories:-

Polymers

Surfactants,

and Fibres.

1.3.1 Polymers

A polymer is a mixture of compounds formed by polymerization, composed of many repeated subunits. Because of their wide range of properties, both synthetic and natural polymers play an important role in everyday life. Both synthetic and natural polymers are made by polymerization of many small molecules known as monomers [3]. These high molecular mass relative to small molecule compounds has unique physical properties like toughness, viscoelasticity and tendency to form glasses and semi-crystalline structures rather than crystals. The different types of polymer drag reducers are shown in Table 1.1.

Table 1.1: List of polymer drag reducers.

S.No	Water-soluble Polymers	Hydrocarbon soluble polymers
1	Poly-ethylene oxide (PEO)	Poly-isobutylene (PIV)
2	Poly-acrylamide (PAM)	Polystyrene (PS)
3	Guar gum (GG)	Poly-methyl methacrylate (PMMA)
4	Xanthan gum (XG)	Poly-dimethyl siloxane(PDMS)
5	Hydroxyethyl cellulose (HEC)	Poly-cisisoprene (PCIP)

1.4 Biopolymers:

Biopolymers are polymeric biomolecules produced by the living organisms, they are eco-friendly and shows great resistance to the mechanical degradation. High molecular weight biopolymers like polysaccharides made up of living organisms influences the drag reduction very effectively. Polysaccharide such as xanthan gum (XG) shows significant resistance to the

mechanical degradation as compared to the flexible polymers with similar molecular weights. Xanthan gum is one of the most commonly used drag reducing biopolymer. Amongst all the polymers polyacrylamide (PAM) shows better shear stability but due to high initial cost it is not widely used [2].

In this study two high molecular weight bio-polymers namely guar gum and hydroxyethyl cellulose are used, purchased from BRP Chemicals Delhi. Guar gum is a non-ionic polysaccharide galactomannan, grade identification can be done on the basis of purity and viscosity. When dissolved in water it forms viscous solution. Non-ionic nature of guar gum is responsible for constant viscosity of solutions in pH range of 1-10.5. The viscosity of guar gum solutions starts decreasing after 48 hours accompanied with the drop in pH due to fermentation. Hence, the master solution prepared for experimentation is used immediately before ageing. Molecular weight of guar gum is found to be in the range of 250,000-950,000. Molecular structure of guar gum is shown in Figure 1.3.

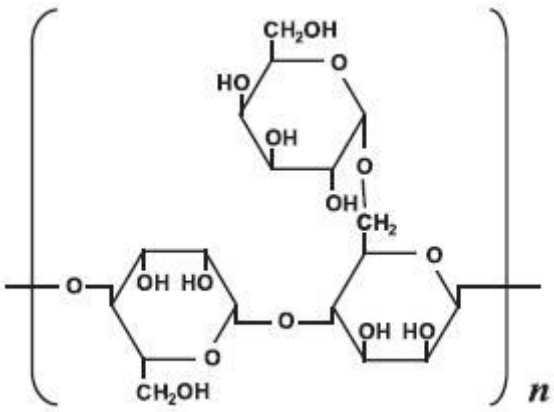

Figure 1.3: Structure of guar gum [3].

Hydroxyethyl cellulose (HEC) is a non-ionic, water soluble polymer, it is white and free flowing granular powder with wide range of commercial applications. It is prepared by etherification of alkali cellulose with ethylene oxide. The pH of hydroxyethyl cellulose (HEC) is found to be above 7 for all the concentrations used in this experimental study. It exhibits excellent shear stability and self-life stability than guar gum. Solutions of high viscosity or high concentration exhibits high degree of pseudo plasticity. At high shear rates molecules get oriented in the direction of the flow decreasing the flow resistance i.e., drag reduction. Average molecular weight of hydroxyethyl cellulose (HEC) is 250000. Molecular structure of hydroxyethyl cellulose is shown in Figure 1.4.

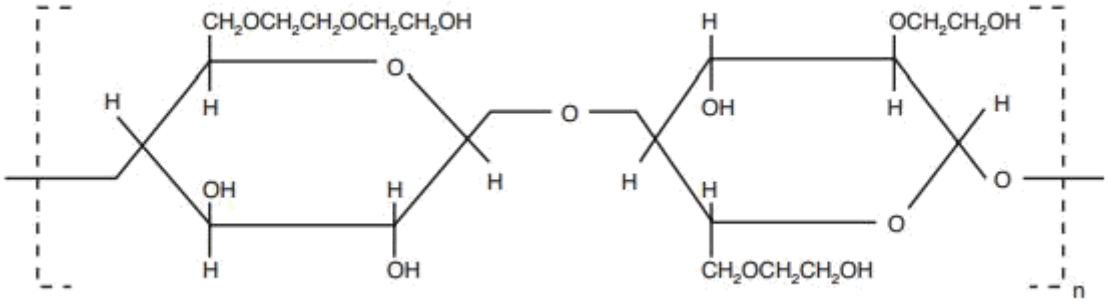

Figure 1.4: Structure of hydroxyethyl cellulose [2].

1.5 Drag Reduction by Polymers

Dissolving a small amount of high molecular weight polymers (few weight parts per million) in a single–phase water flow at high Reynolds number significantly reduces the pressure drop in the pipe. This effect was first discovered by Toms in 1949. This phenomenon has received a lot of attention thereafter, due to its wide range of practical applications. Even though the polymers are active on a smaller scale, they influence the macroscopic scales of the flow which determines the drag to great extent.

For the past couple of years, numerous numerical and experimental studies has been carried out on polymer induced drag reduction in turbulent flow in a pipe. Virk [4] from his experimental study, summarized his results for different flow regimes. He showed that there is no drag reduction at low Reynolds number (laminar flow) and in the turbulent regime there is a considerable amount of drag reduction. He presented experimental evidence that drag reduction is limited to an asymptotic value known as maximum drag reduction (MDR) asymptote. A detail study of drag reduction phenomenon is given by Gyr and Bewersdorff [5]. Warholic, Massah and Hanratty [6] characterized two distinct regimes low drag reduction (LDR) and high drag reduction (HDR) in which LDR exhibits almost similar statistical trends to Newtonian fluid. At drag reduction above 40%, flow enters the HDR regime in which Reynolds shear stresses are very less or negligible. Lumley [7] described the changes in the turbulence structure is due to the stretching of randomly coiled polymers because of strong turbulent flow leads to increases flow rate i.e., drag reduction.

In recent studies many numerical simulations were performed to relate turbulence and polymer stresses directly. Many explanations were proposed for the mechanism of polymer induced drag reduction through such computations. Most of these studies were relied on time and space averaged statistics. Min [8] analyzed their simulation on the basis of elastic energy

observing remarkable transport of energy from sublayer to buffer layer and logarithmic region. Ptasinski [9] tried to relate damping of vortices with shear effect in the near wall region which decouples the outer and inner layer vortices effectively. Sureshkumar [10] presented the results of direct numerical simulation (DNS) of polymer solution where polymer chains are modelled as finitely extensible non-linear elastic (FENE-P) dumbbells.

In all the experimental studies discussed above, low concentrations polymer solutions are injected in the turbulent pipe flow. In this study high concentration bio-polymers (guar gum and hydroxyethyl cellulose) are injected at high Reynolds number and observed the changes in the pressure drop across the pipe (test section) and compared to the Newtonian flow (water). All the results are close to maximum drag reduction (MDR) asymptote or Virk's asymptote. Mechanical degradation rate at different concentrations and Reynolds number and properties like pH and viscosity are also calculated for all polymer concentrations.

1.6 Applications

The drag reducing polymers (DRP's) has a wide range of practical applications. Few of the applications are discussed below.

Drag reducing polymers (DRP's) were used to increase the flow rate of crude oil in the Trans-Alaska pipeline system where only 1ppm drag reducer increased the flow rate by 33% is the best known practical application [11]. Another similar application is found in the Oseberg field in the North Sea in which drag reducing agents are used in the petroleum pipeline installations Burger et al. [12].

Use of DRP's in sewage system and flood water drains to increase the flow rates are much cheaper than construction of new pipe lines.

Drag reducing polymer additives can also be used in the transportation of high weight solids like coal, sediments, ash etc. by pipelines with less pumping power costs compared to the conventional methods [13].

This phenomenon can also be used in the military applications, like increasing the velocity of underwater bodies like submarines and torpedoes. Even 20% of drag reduction may increase the speed by 6.8% [14].

For the past couple of years drag reducing polymers (DRP's) are used in the biomedical industries, one such application is treatment of circulatory or cardiovascular diseases [15].

Drag reducing additives has been used in large scale in District heating cooling systems (DHC) have lowered the pipe flow energy significantly [16].

Drag reducing polymers (DRP's) shows longer effectiveness in the disk pump applications, due to low mechanical degradation rate.

Ice slurry systems showed improved performance using drag reducing polymers in the cold heat storage, transportation and heat exchange systems, bearing close relationship between drag reduction and energy conservation [17].

1.7 Advantages

The various advantages of drag reduction by polymers are as follows:

Reduces the pump capacity.

Reduces the power consumption.

Longevity of the pipes.

Improves the capacity of fire hoses.

Useful in shipbuilding industry.

Reduces the transportation cost

Low consumption of polymers(in

ppm) Do not contribute to pollution.

Bio-polymers are less expensive.

1.8 Disadvantages

The disadvantages in polymer induced drag reduction are as follows:

Selection of proper polymers is very

important. Polymers are costly.

Difficulty in knowing the exact concentration of polymers to be

injected. Degradation of polymers at high temperature and pressure.

Chapter 2
Literature Review

Many researchers have given their own interpretation or theories regarding the phenomenon involved in polymer induced drag reduction. In this chapter the main focus is to understand these suggested theories and research work done in this area.

2.1 Suggested Theories

There are many theories suggested to explain the mechanism involved in polymer induced drag reduction in the turbulent flow in the pipe.

1. Lumley theory

Lumley [18], described the phenomenon involved in the drag reduction as 'Molecular Extension'. The randomly coiled polymer chains stretches due to high shear rates of strong turbulence, outside the viscous sub layer. Due to this the effective viscosity increases in the turbulent regime, but the viscosity in the viscous sub layer remains less. This high effective viscosity increases the thickness of viscous sub layer and thus reduces the drag. Thus, the onset of drag reduction can be observed when the relaxation time of polymers is more than the time scale of turbulence.

2. Hinch theory

Hinch [19] studied the extended state of randomly coiled macro-molecules. He considered different models, showing the significance of inextensibility of the polymer chains and variation of the coefficient of friction with the extension. In 'Elastic ellipsoidal model', he interpreted the dependence of polymer chain stretching due to strong turbulence on the distortion. With increase in distortions the frictional intensity of the flow increases. Large distortions in the strong flows grows until they are limited by finite extensibility of the polymer chains. In 'Inextensible flexible thread model', he considered the effect of hydro-dynamic stretching and inextensibility of flexible polymer threads. The inextensible thread starts straightening from S shape, initially it tends to an orientation in which it is in tension and then it snaps the thread straight. In 'Transversely diffusing thread model', he suggested weak motions acting on the straight thread will cause transverse distortions on a small scale which is described by the diffusion process in the deformation space. Due to high degree of tension at

the ends of the thread the transverse displacement is less as compared to the center. In association with transverse distortions, due to small coiling effect the ends of the flexible thread comes closer when it is not straight. Weak flow strength is required to maintain the stretched polymer as compared to the flow required for the large distortions of randomly coiled chains.

3. Landahl theory

Landahl [20], has implemented a "two scale' model to understand the mechanism of polymer induced drag reduction. This model was proposed to study the effect of local turbulence on large scale. This small scale motion is produced by the secondary inflectional instabilities, which is considered as the driving mechanism for the large scale with generation of local Reynolds stresses. Through this model, drag reduction due to the additives of different kinds appears more easily explained as it is caused by the stabilization of inflectional velocity profile due to additives.

4. Yo-Yo theory

The conical channel system of the polymer solution was investigated theoretically, introduced by Ryskin [21]. Yo-Yo model states that elongation of macro-molecules elongates under the straining action of strong turbulence. It introduces the additional elongation of viscosity that enhances the thickness of viscous sub-layer which reduces the drag. This model observes the large polymer effect in the transient deformation of macro-molecules due to the extensional flow. These elongating macro-molecules increases the extensional viscosity in turbulence.

5. Gennes theory

Gennes [22], introduced unique model in which the effect of polymers was explained by elastic modulus in small length scales, suggesting that elasticity of polymer chains are responsible for drag reduction. Dilute polymer solution enhance s the viscosity in the flow. Cascading at each distance y from the wall, it is truncat ed elastically giving the law for eddy size with respect to distance y. They behave elastically in the strong rapidly varying shear fields. Thus the turbulent cascade system must be modified, when the elastic stresses are comparable to Reynolds stresses. The main idea of this model is, dilute flexible polymer chains behaves elastically at high frequencies. The Kolmogorov cascade system remains undisturbed by polymer additives up to certain value where polymer stresses balances the Reynolds stresses. This appears at full stretching of flexible polymer chains and viscous effects are dominant.

6. Gyr and Bewersdorff theory

The assorted drag reduction phenomenon, was first observed in 1970's [23]. The experiments reveal that injections location strongly influence the drag reduction. Three different positions were obtained in a rectangular channel which are equally located from one another and from the wall. It was observed that with single injection point drag reduction is extremely low as compared to the other injection points with same polymer concentration. This can be explained by the fact that l/d ratio (where l is downstream distance from the injector and d is the diameter of the pipe) in span-wise direction is not sufficient to reach MDR value. For the remaining two injectors, the span-wise distance from first injector to the wall and center of the channel is same. It is consistent with the view that polymer threads coming out of the injection tip directly interacts with the large scale structures in the region of its influence. It is assumed that in homogenous drag reduction, presence of active polymer chains in the buffer region are responsible for the drag reduction.

Two main effects were suggested from the experimental results related to assorted or heterogeneous drag reduction: small amount of polymers are transferred from the thread to the fluid and the resulting effects are similar to the drag reduction of homogenous drag reduction. In other results, the visco-elastic thread interacts with the bulk flow. Hence, heterogeneous drag reduction occurs due to small amount of dilute polymers in the near-wall region interacting with the turbulence. Though the mechanism involved in this interaction is not clear, but it is assumed that some kind of self-induced forcing suppresses the Reynolds stresses and can be realized in the core of the flow.

2.2 Literature Review

This section will give an idea about the research work done in this area. The main focus of this literature review will be on the behavior of polymers at different temperature and concentrations in turbulent flow.

Ptasinski [9] performed the Laser Doppler Velocimetry (LDV) experiments in polymer induced turbulent pipe flow. In this experimental study Superfloc A110 (hydrolyzed polyacrylamide) was used as polymer additive, and conditions were close to MDR or Virk's asymptote. Amount of drag reduction was observed in terms of change in friction factor as a function of wall Reynolds number. Wall Reynolds number is used following the fact that for

non-Newtonian fluids the viscosity does not have a constant value. It is based on an introduction of wall viscosity related to wall shear stress.

All the LDV experiments were performed at Re=10000, showing high rate of drag reduction. The results obtained are compared with the results obtained with water and also with the very dilute solution exhibiting very small amount of drag reduction. The polymers contributes significantly to the total stress. An increase in the slope of logarithmic profile and thickening of buffer layer is found with respect to the mean velocity profile. It is also found that for streamwise velocity fluctuations, root mean square increases for low polymer concentrations but returns to the values comparable to those of water at high concentrations. Reynolds stress and correlation coefficient of streamwise and normal components drastically reduces over the entire pipe diameter. Reynolds stress are non-zero at maximum drag reduction (MDR). The reason for decrease in the Reynolds stress is large polymetric stress which can be around 60% of the total stress. The kinetic energy of turbulent flow shows a possible negative polymetric dissipation of turbulent energy.

Virk [24] has done the physical interpretation of polymer induced drag reduction in the turbulent pipe flow. The turbulence-polymer interactions that are responsible for the drag reduction commences near the plane of peak turbulent energy production, suggesting that randomly coiled polymer molecules influences the turbulent bursting process. In the region near the onset of drag reduction, the duration of a turbulent burst is of the order of relaxation time of the macro-molecule, and just after the onset, the extent of drag reduction is related to the turbulent strain energy of dilute polymer solution. Therefore, these observations suggests that the polymer chain extension is involved in the drag reduction mechanism. The radius of gyration of randomly-coiled macromolecule is smaller than 10^{-3} times the turbulent burst length scale. The radial and axial flow fields are decoupled near the region of interaction, as experienced by a striking reduction in the u-v ***c***orrelation coefficient, relative to Newtonian. The decoupling of polymer induced turbulent flow fields seems to retard about the radial transport of axial momentum and turbulent kinetic energy. The drag reduction observed is possibly a consequence of the rearrangements, with an increase in maximum kinetic energy that the inner flows that maintains the overall cross-sectional turbulent energy balance. The data for maximum drag reduction (MDR) is plotted in f versus Re graph shown in Figure 2.1.

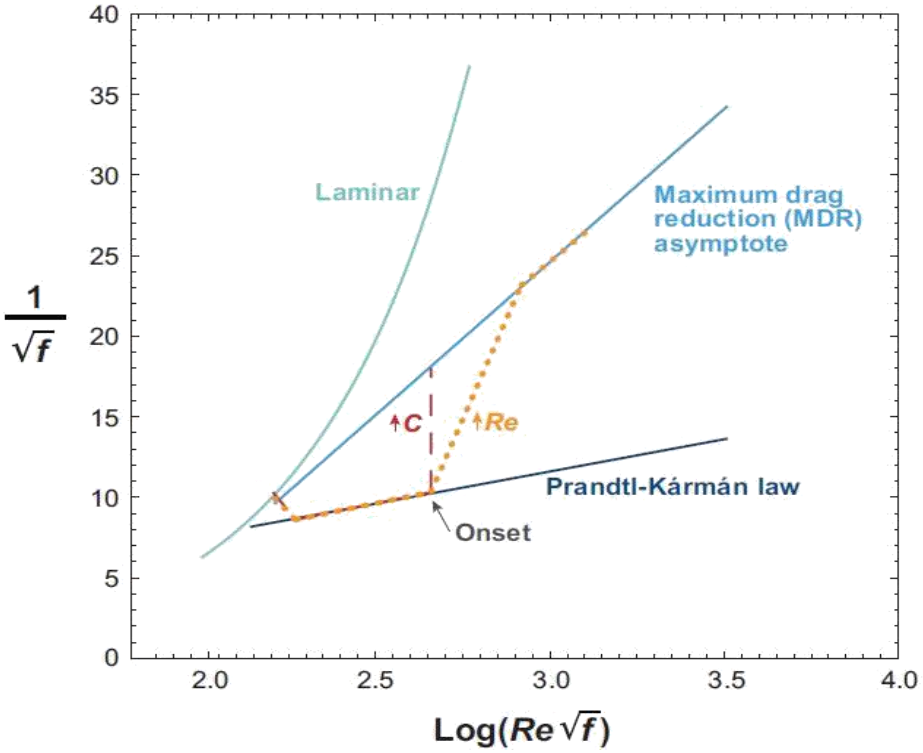

Figure 2.1: Representation of the data for maximum drag reduction in the f versus Re plot [24].

Li et al. [25] performed direct numerical simulation of drag reduction by polymers in the turbulent channel flow. FENE-P and Oldroyd-B models were applied to evaluate the polymetric chain dynamics. In this study it is shown that for high percentage of drag reduction, polymer chain extensibility and high Weissenberg number is required. These results are used to develop a scaling describing the interplay between maximum polymer chain extensibility and relaxation time, and also the extent of drag reduction rate as a function of Reynolds number. In addition to this the turbulence statistics were also analyzed and the correlations between polymer body forces and velocity fluctuations were obtained with particular emphasis on high drag reduction (HDR) and maximum drag reduction (MDR) regimes. The results shows that there is a positive relation between the polymer body force in the near wall region and stream wise velocity. It also indicates that stretching polymer chains extracts energy from the flow, reducing the turbulent fluctuations. The results suggests that there is an intricate balance between average rotation speed of axial vortices near the wall and elastic forces, which is the measure of Reynolds stress production.

Abubakar et al. [26] studied about the parameters of polymers helping in the drag reduction and their performance in the turbulent pipe flow. The effect of parameters such as molecular

weight, charge density, and chemical structure on drag reduction rate was investigated using a single-phase water flow at high Reynolds number in a horizontal pipe. Drag reduction increases significantly with polymer concentration of 10 ppm and above this it reaches the plateau. The drag reduction rate increases with the increase in polymer molecular weight at the plateau region. The charge density should be optimized, since increase above a certain value would make the polymer structure more rigid lowering its drag reduction capability. It has been also found that drag reduction is not a function of the intrinsic viscosity, indicating the hydro-dynamic volume of the polymer in aqueous solution. This study also suggests that there is a need of both elasticity and ability of the polymers to form intermolecular associations, which can be enhanced by increasing the molecular weight and decreasing the charge density to perform as a good drag reducer. The variation of drag reduction percentage with different concentrations of AN105-SH is shown in Figure 2.2. The variation of drag reduction percentage depending on charge density and molecular weight of polymers is shown in Figure 2.3.

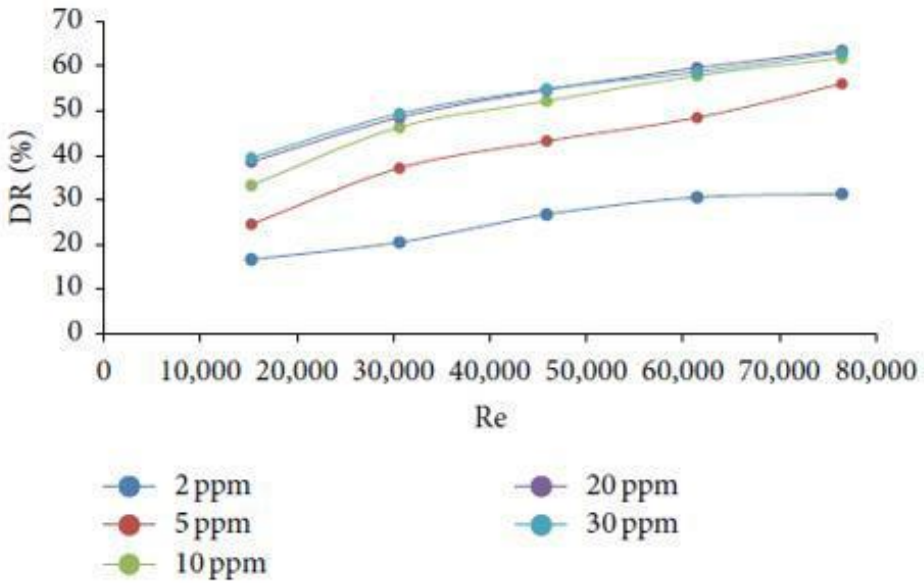

Figure 2.2: Drag reduction dependence on Reynolds number at different polymer concentrations for AN105-SH [26].

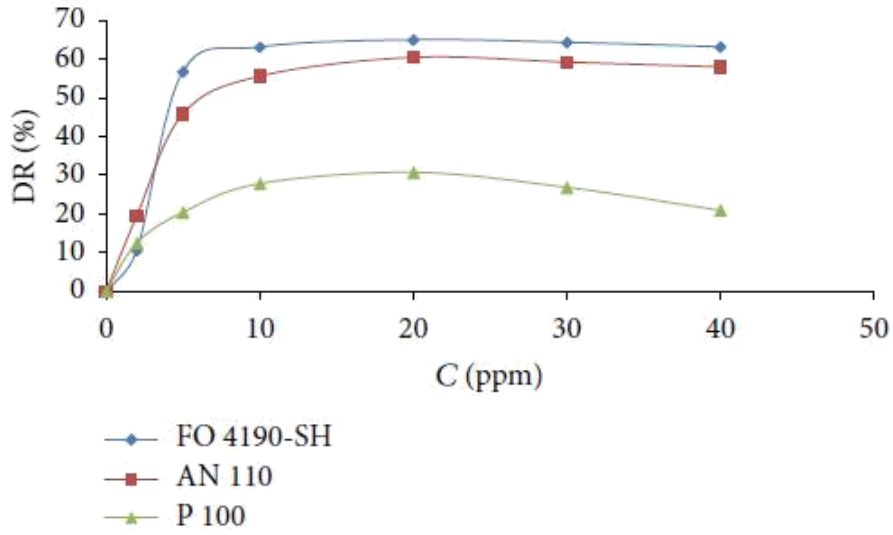

Figure 2.3: Comparison of drag reduction of nonionic, cationic and anionic polymers of the same charge density and molecular weight. [26]

Warholic et al. [6] has studied the effects of concentration and mixing of polymers (DPR's) on turbulence. The Reynolds shear stresses are approximately negligible across the entire cross section of the channel for the flows close to maximum drag reduction (MDR). By considering the energy balance, the turbulence at MDR is produced by the fluctuating polymetric stresses. The velocity profile obtained under MDR does not have the parabolic profile observed for the Newtonian laminar flow.

It is observed that for the maximum drag reduction, the near wall vortices sustaining the turbulence in a Newtonian fluid are destroyed. Hence, the velocity field is somewhat different from the classical turbulence, produced by the interaction between the polymer additives and fluctuating flow field.

From this study it is discovered that the rate of drag reduction mainly depends upon how the polymers are added, and this effect was observed for the polymer concentrations as low as 0.25 ppm. This result is interpreted as the effectiveness of the drag reducing polymers (DRP's) depends on the presence of aggregates in the aqueous solution. These aggregates needs to be break up irreversibly to be consistent with experimental measurements. This interpretation gives a theory to explain polymer degradation and the effect of chemical composition of the solution. The polymer aggregates appears intermittently, so it is difficult to understand the effect on velocity field at such small concentrations. It also illustrates that the near wall vortices regenerates themselves by certain process which is followed by several generations. From the

change in local turbulence due to the destruction of the vortices while interacting with the polymer aggregates much stronger impact can be expected.

Dubief et al. [27] performed numerical simulations on polymer solution in a turbulent flow using the FENE-P model to characterize the effect of polymers on turbulent structures. The polymers stores and releases energy to the flow in a systematic manner. The energy is stored in the near wall vortices was anticipated for a long time, but quite unexpectedly the coherent energy were observed in the near wall region. The fluctuating polymetric work is shown to re-energize the reducing stream wise velocity fluctuations in the high velocity streaks just above the viscous sublayer.

The drag reduction and turbulence intensifying properties of polymers are related to the coherent structures. Polymer influences the near wall vortices and enhances the kinetic energy of near wall streaks. The net balance of these two opposite actions leads to drag reduced turbulent flow. Hence, the study on polymer work characterizes when the polymers are more likely to release the energy into the near wall streaks. This phenomenon is related to the region where kinetic energy decreases in absence of polymers. The release of energy from the polymers in this region counteracts the viscous effects which occurs after the polymers resides in the streaks but not when they are transported from buffer region to the streaks through downwash flows by the vortices. The damping of turbulence takes place in the flows generated by the vortices, since upwash and downwash flows occurs around the vortices with the preference of upwash events because of pre-stretching of the polymer chains by high shear close to the wall. Hence this mechanism of drag reduction by polymers is represented as the modified regeneration cycle of wall turbulence shown in Figure 2.5.

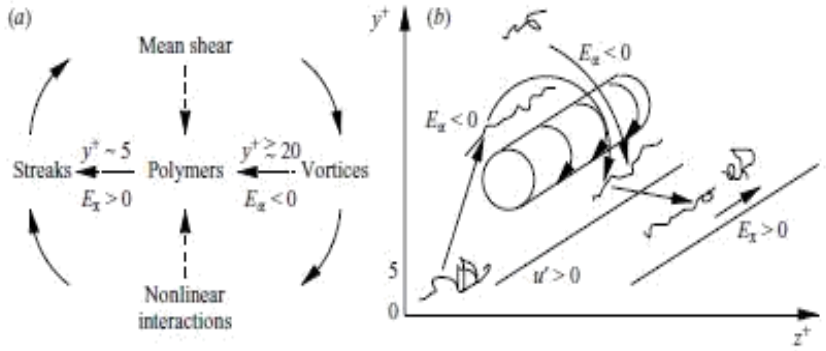

Figure 2.4: (a) Cycle of wall turbulence regeneration with energy transfer from the polymers to the flow, (b) Vortex pumping fluid from the near-wall region and creating turbulence damping polymer work [27].

Toonder et al. [28] has examined the role of elasticity and stress anisotropy in the mechanism of polymer induced drag reduction in a turbulent pipe flow using direct numerical simulation (DNS) and laser doppler velocimetry (LDV). In this study they considered two models to illustrate the effect of polymers in the turbulent flow. The first model is based on the theory of elongated particles in the Newtonian fluid that models the viscous anisotropic stresses due to the polymer chain stretching. Second model is the extension of previous one with an elastic component that can be described by anisotropic maxwell model. They observed thickening of buffer layer in the drag reduced flow and corresponding offset in the logarithmic region. The peak value of axial rms profile increases and shifts away from the wall but in other directions as its value decreases. No proper evidence for Reynolds stress deficit is found in DNS. The changes due to the viscous anisotropic model is mainly due to the presence of normal stress in the axial direction. The turbulence in the axial direction is distributed from smaller to larger scales. The radial velocity fluctuations are damped over the entire wavenumber spectra near the wall. It is also shown, the stretching characteristics are altered by the viscous anisotropic model, positive and negative deformations are suppressed. The negative stretching is suppressed much strongly as compared to positive stretching.

Another DNS was performed using the anisotropic model to test de Gennes hypothesis, it was interpreted that the extension of viscous anisotropic stress with an elastic component. Their results confirms the hypothesis of Lumley (1969) that stretching of polymer chains are responsible for drag reduction but not with the increasing viscosity proposed by him. On the basis of their results they proposed that in the mechanism of polymer induced drag reduction viscous anisotropic stresses play an important role.

Graham [29] studied the polymer induced drag reduction phenomenon also known as the "Toms effect". The rate of strain near the wall is much larger than the polymer relaxation rate, polymer chain stretches in the near-wall streaks and do not relax until they enter the quasi stream wise vortices until they suppress them. It is these stream wise vortices in the buffer layer that drive convective momentum transport; suppressing them leads to drag reduction. The strength of these vortices decreases which leads to redistribution of Reynolds stresses, resulting in changes in the velocity fluctuations of the buffer layer. It seems likely that a related mechanism is involved in the log layer, as also the mean shear flow tilts and stretches the vortices into the mean flow direction. As the strain rates are lower here, the polymers are not highly stretched and their influence is weaker than the buffer region.

Bark et al. [30] performed a practical experiment on drag reduction in the turbulent flow due to polymers on Euromech-52, they came up with the conclusion that the research on polymer induced drag reduction should aim at first order and second order phenomenon. In 'First order' phenomena, large reduction in skin-friction drag is achieved with small amounts of polymers. And in 'Second order' phenomena, the effects of polymer degradation is of great practical importance, and to understand the mechanism involved in drag reduction. Similar opinions were shared by other participants as well, they considered the most desirable directions for research in the two problem areas central to the drag reduction phenomenon, namely turbulence structure and the rheology of suspensions.

The practical aspects of drag reduction were not forgotten at Euromech-52**.** They conducted drag reduction experiment by pouring polyethylene oxide into the sea at the bow of the steamer. The participants noticed a definite increase in the speed of the ship which was also confirmed by the ship's captain.

Ali et al. [31] performed experimental investigation of polymer induced drag reduction in flowing crude oil, which could increase the pumping capacity of crude oil over long distances. In their study two types of crude oil namely, Karkok crude oil and Basrah crude oil are used.

Three types polymers with high molecular weight namely poly isobutylene PIB150K, PIB90K and poly isoprene (PIP) are used, the polymers are injected through pumping system at different concentrations rounded between (10-50) ppm with temperatures range of 30˚C to 50˚C. They performed several experiments to determine the best concentration of polymer which satisfies the lowest drag force on crude oil flow rate .The results show that the best

execution are realization for PIB150K at 30 ppm and 45˚C for two types of crude oil it is shown in Figure 2.6 and 2.7.

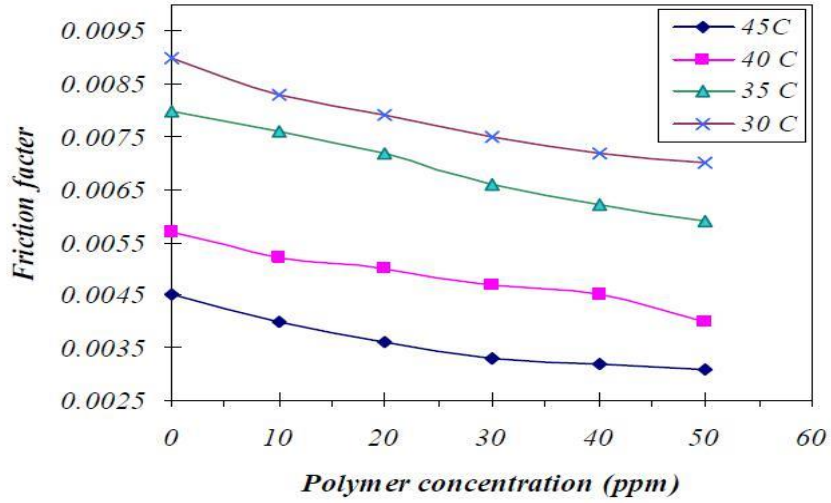

Figure 2.5: Effect of polymer concentration on the friction factor of Kurkuk crude oil [31].

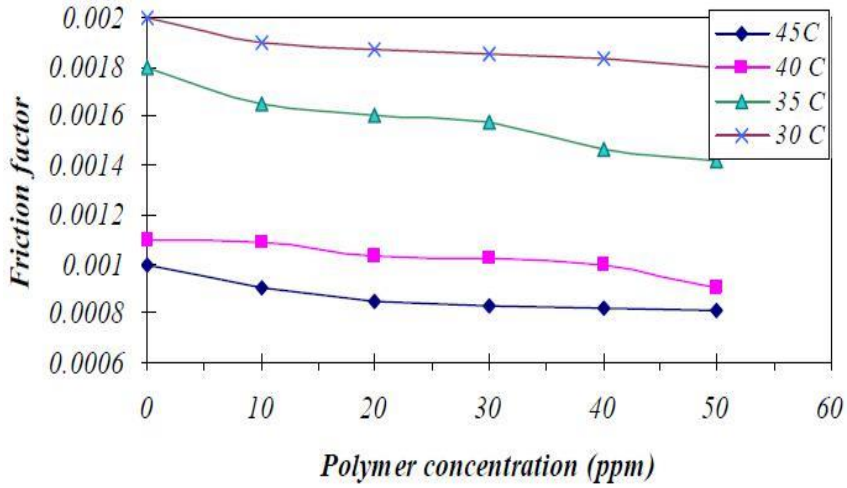

Figure 2.6: Effect of polymer concentration on the friction factor of Basrah crude oil [31].

From the experimental results they have concluded that best concentration for PIB150K for maximum drag reduction is 30ppm when added to Kurkuk crude oil at 35ºC reducing the draf force by 22.23% for velocity of 1.85m/s. Same concentration when added to Basrah oil at 45ºC reduces the drag force by 20.3% at 45ºCfor velocity of 6.65m/s. The friction factor gradually decreases when the polymer concentration increases. The performance of the polymer is better for light crude oil than heavy crude oil.

Kim et al. [32] examined the effects of polymer stresses in the fully developed turbulent structures using DNS. They used two point spatial correlations and linear stochastic estimation for finding the patterns of vorticity, polymer torque, velocity, and polymer force in the conditional eddies. Both low drag reduction (LDR) and high drag reduction (LDR) regimes are investigated and compared with the results of Newtonian fluid and for computation the conditional averaged near wall eddies, linear stochastic estimation were employed. It is shown that the near wall turbulent structure are depleted and prolongate in streamwise direction due to the polymetric stresses. In this study the averaged conditionally fields are responsible for the events concerned with huge contribution to the polymetric work are also examined. This study explains vortex retardation by the polymetric forces in the fully developed turbulent flow by relating the 3-D structure of eddies to the structure of polymetric forces. In more detail, the torque due to the polymer stress opposes the vortex rotation are responsible for their weakening. The simulations also shows that the total number of vortices in the drag reduction flows are also reduced and also some part of reduction in Reynolds stress. Hence these results offers an explanation of possible mechanism of polymer induced drag reduction in the outer region of wall turbulence and also in the buffer region.

Tian et al. [33] studied the rheological properties and drag reduction by xanthum gum (XG) and hydroxypropyl xanthan gum (HXG) solutions in a smooth tube. Hydroxypropyl xanthan gum (HXG) is prepared from xanthan gum and propylene oxide under the alkaline conditions. The rheological properties of aqueous HXG and XG dilute solutions with different concentrations were studied. The honeycomb network of aqueous HXG and XG solutions were investigated by Cryo-FESEM. The images generated by Cryo-FESEM shows that aqueous HXG solution has much stronger honeycomb structure than the XG solution.

The apparent viscosity and visco elasticity of hydroxypropyl xanthan gum (HXG) solution was increased and also the network was further strengthened, through the hydroxypropyl modification under alkaline conditions. Both, xanthan gum and hydroxypropyl xanthan gum shows significant shear thinning property which is described by the Ostwald Dewaele equation.

From the experimental study, for 1 g/L (1000ppm) concentration of both the polymer solutions, the maximum drag reduction percentage in the smooth pipe reached 72.8% for HXG and 68.1% for XG, it is shown in Figure 2.8. Hence HXG solutions reduces the pressure drop across the pipe and increases the flow rate significantly. Therefore, HXG can be treated as a new drag reduction polymer.

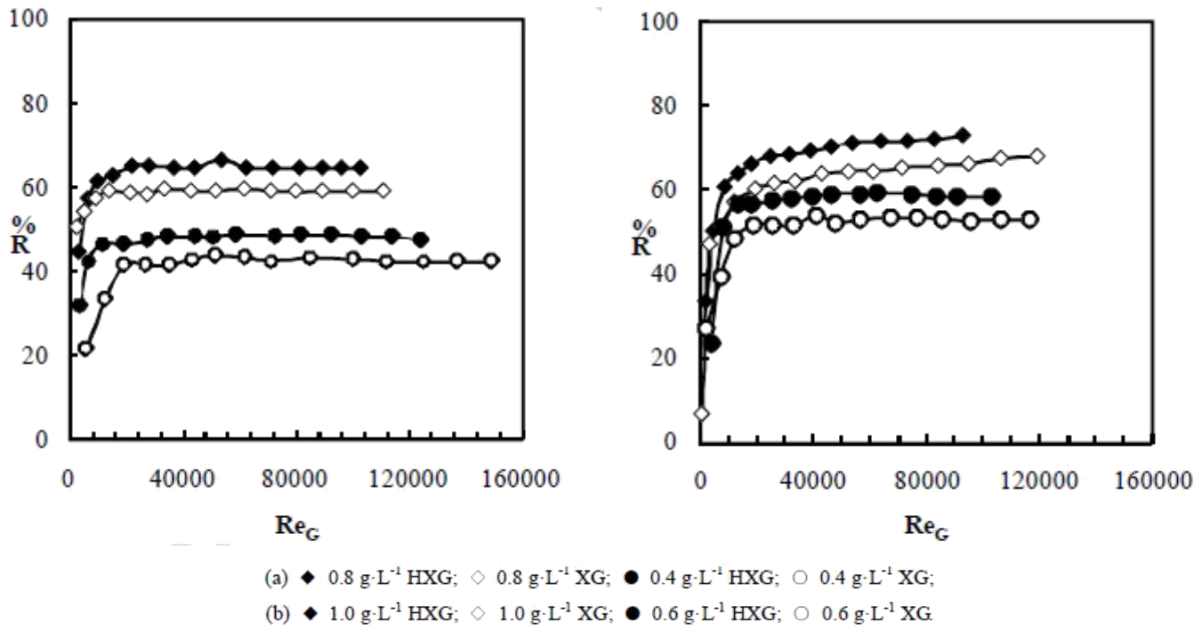

Figure 2.7: Drag reduction as a function of Reynolds number for aqueous solutions of HXG and XG with different concentrations [33].

Terrapon et al. [34] examined the phenomenon of polymer induced drag reduction in a turbulent pipe flow by Brownian dynamics simulations. The dynamics and trajectories of polymer chains were investigated in the turbulent channel flow. In this study they used FENE, FENE-P and multimode FENE models are used with different parameters for investigating the mechanism involved in polymer stretching. Different flow types are characterized according to their topologies. From their topological analysis they have concluded that polymer molecule stretches only if it experiences a flow with strong extensional character. They introduced a quantity σ^* to measure the flow ability to stretch the polymer molecule. From the flow visualizations it is found that the regions with large σ^* are found close to the near wall vortices and also seen that these structure are greatly affected by the mean flow, illustrated in Figure 2.9.This correlation between $\sigma^*$and vortices gave a new insight to the mechanism of polymer induced drag reduction. A wide range of Weissenberg number were also investigated and was found that polymer chains stretches in the near wall region next to the vortices due to the straining flows. At low W_i the polymer chains stretches due to the strong biaxial flow, whereas at high Wi only the bursts of strong biaxial flow can fully extend the polymer chains. Hence it was concluded that these bursts of the biaxial flows constrained by the flow topology occurring before the maximum extension of chain are the primary reason for the polymer chain stretching mechanism.

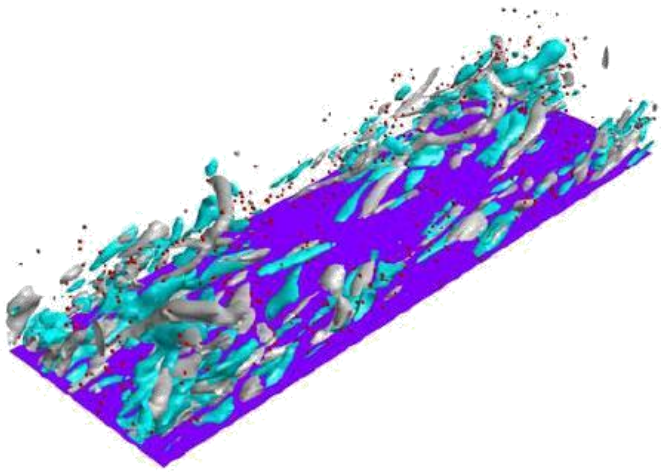

Figure 2.8: Instantaneous view of lower half of the channel representing the vortices and polymer molecules in red [34]

Petrie et al. [35] performed experimental study on the effect of surface roughness on polymer drag reduction in a flat plat turbulent boundary layer at zero pressure gradient. In this study they considered both slot injected polymer and homogenous polymer ocean cases in wide range of flow conditions as well as surface roughness. In this study, they measured skin friction drag reduction and found 60 % of drag reduction for both homogenous and injected cases with rough surfaces. To achieve higher percentage of drag reduction, higher polymer concentration is required for the homogenous case if the roughness is more. The percentage of drag reduction decreases to very low values quickly with the increase in surface roughness when the freestream velocity is increased. It is observed that the percentage of drag reduction is more on the rough surface with polymer injection as compared to the smooth surface. From their experimentation it is observed that in some conditions with polymer injection the skin friction drag on the rough surface is less than the drag force on smooth surface under comparable conditions.

Omrani et al. [36] performed experimental study on the effect of Coriolis force in polymer induced drag reduction in a turbulent pipe flow. In this they used a smooth pipe of 25 mm diameter on a horizontal table rotating about the vertical axis. This rotation is made dimensionless to form Rotation number (Ro) with friction velocity and pipe diameter. The pressure drop is measured between the two different Reynolds numbers 15000 and 30000 for a range of bulk rotation number between 0 to 0.6 from which average friction factor f is calculated. The friction factor (f) changes with the rotation number for the single phase flow,

these results match qualitatively with the square duct flow. It is found that the effect of rotation and polymer seems to be super positional in the regime of drag reduction with polymers and remains unaltered by the rotation. It is now inferred that large scale secondary flow caused by the rotation doesn't influence the near wall phenomenon causing polymer induced drag reduction.

Summary

The phenomenon of drag reduction by polymers has gained the attention of many researchers ever since its invention in 1949. Since then lot of research has been carried out with synthetic polymers which are very expensive as compared to the bio-polymers. In this study two different bio-polymers guar gum and hydroxyethyl cellulose are used, which are ecofriendly and has better shear stability than the synthetic polymers. They enhances the durability of drag reduction additives in the entire process.

In this experimental study, the pressure drop across the pipe section using gaur gum (GG) and hydroxyethyl cellulose (HEC) at different Reynolds number and concentrations are calculated. The effect of mechanical degradation due to the centrifugal pump is also observed at different concentrations and Reynolds number. The results obtained are further validated with universally applied maximum drag reducing (MDR) asymptote suggested by Virk.

CHAPTER 3
Methodology

In this chapter the details of experimental setup and different parametric conditions are discussed. The various equations used for designing the setup and experimental calculations are also given.

3.1 Experimental Study

From literature, it is found that lot of research have been done in the domain of drag reduction in the turbulent flow using polymers. Injecting small amount of polymers in the Newtonian fluid like water significantly reduces the fluid resistance in the flow. In present work, two bio-polymers were used to investigate the effect on drag reduction in the turbulent flow. All the experiments were conducted under ambient temperature (25±0.5) ºC. Photographic view of the experimental setup prepared for experimentation is shown in Figure 3.1.

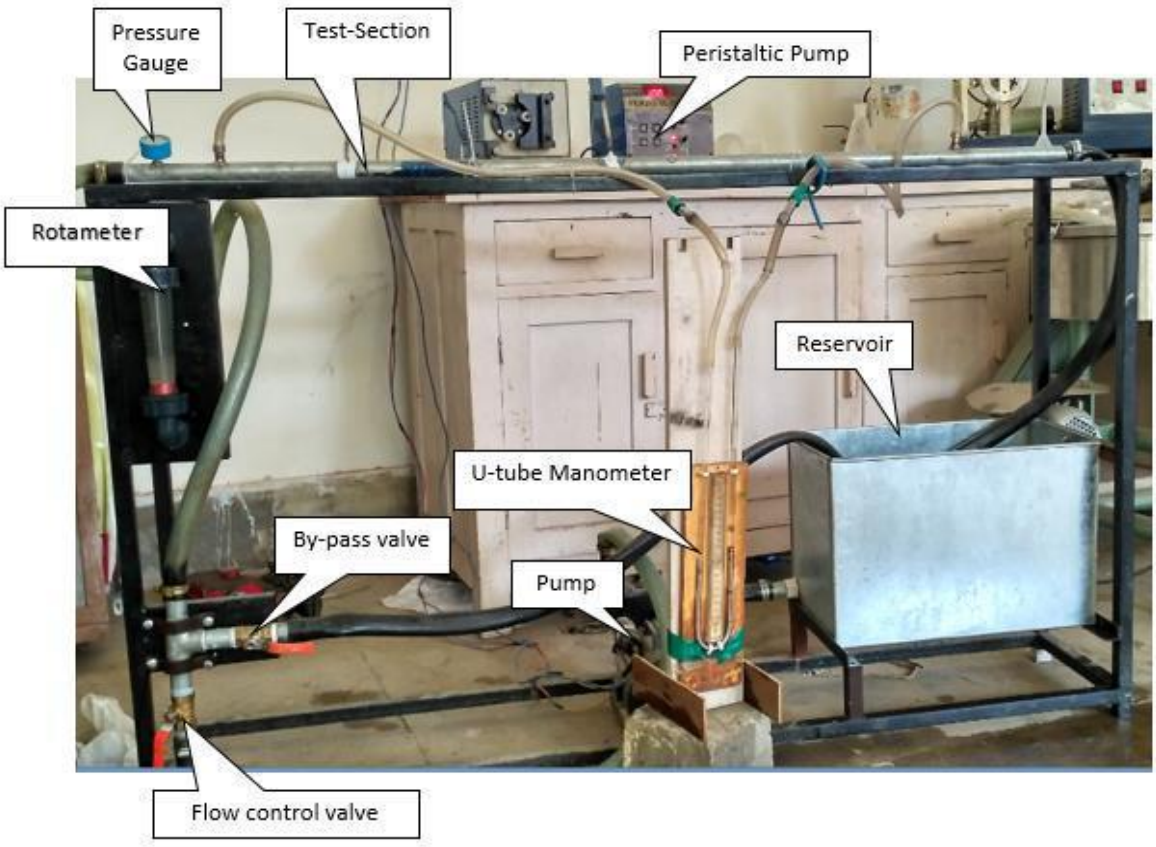

Figure 3.1: Photographic view of experimental setup.

3.2 Layout of Experimental Setup

The setup consists test section of galvanized iron pipe of 1524 mm long and 19 mm inner diameter (ID). The pressure difference with U-tube manometer across the pipe at different flow rates of Newtonian fluid water is noted without drag reducing polymer (DRP). The flow rate is controlled by a by-pass valve connected just below the rotameter. Now, the homogenous solutions of polymers of different concentrations are injected near the wall of the pipe with the help of peristaltic pump at a constant rate of 450cc/hr. The pressure difference across the pipe is measured again with drag reducing polymer (DRP) for different flow rates.

The experimental facility has been fabricated to investigate the effect of bio-polymers in the fully developed turbulent flow. The setup was indigenously designed and fabricated in Thapar University, Patiala, India. The different parametric conditions of experimentation are given in Table 3.1. The schematic diagram of the experimental setup shown in Figure 3.2.

Table 3.1: Various parametric conditions of experimentation.

Parameter	Unit	Test condition
Base fluid	-	Tap water
Bio-polymers	-	Guar gum (GG), Hydroxyethyl cellulose (HEC)
Pipe material	-	Galvanized iron (GI)
Concentration	ppm	1000,1500,2000,2500,3000
Master solution inlet temperature	°C	Ambient temperature (25)
Master solution inlet velocity	cc/hr	450
Water inlet temperature	°C	Ambient temperature (25±0.5)
Water flow rate	LPM	16, 20, 24, 28, 32, 36, 40

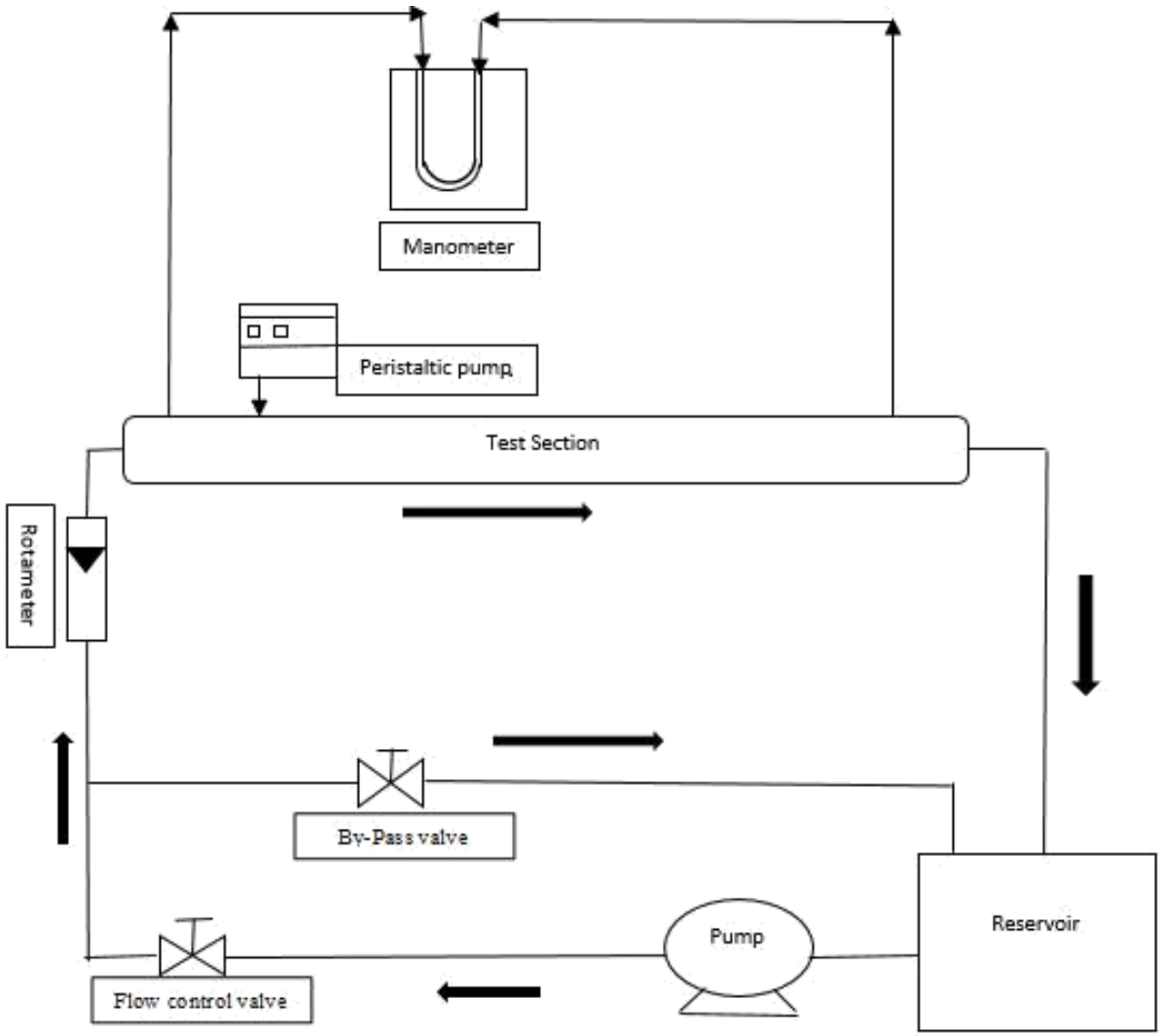

Figure 3.2: Schematic Diagram of Experimental Setup.

3.3 Specification and function of various parts of the experimental setup parts

1. **Reservoir or storage chamber:** Reservoir of 25 liters capacity and made of stainless steel is used to store and circulate the water through the test section. It is properly designed, so that there is no air suction or leakage near the outlet of the reservoir.

2. **Centrifugal pump:** The Centrifugal pump is placed next to the reservoir to circulate water through the test section. The technical specifications of the pump are given in the Table 3.2.

Table 3.2: Specification of the pump.

Type	**Centrifugal**
Power Rating	0.5 HP
Voltage	240 V, 1-PH, 0.5Hz
Size of Outlet Nozzle	1 inch
Maximum Flow Rate	2400 LPH
Maximum Head	6 m

3. **By-pass valve:** It is connected just below the rotameter to control the water flow rate by allowing the excess water back to the reservoir. It is used to maintain the parametric flow rate in the test section.

4. **Rotameter:** The flow rate through the test section is measured with the help of rotameter. The variable area flow meter has float, uniformly tapered tube and a measuring scale. The float is guided by the cylindrical tube. The fluid enters from the bottom and the float rises. Readings on the measuring scale corresponding to the float cap position gives the flow rate in LPH and LPM.

Calibration of rotameter: The rotameter used in the experimentation is calibrated before performing the experiments. For calibration a measuring beaker and a stop watch was used. Different flow rates i.e. 16 LPM, 20 LPM, 24 LPM, 28 LPM, 32 LPM, 36 LPM and 40 LPM are fixed on the measuring scale, which is scaled in LPM as well as in LPH and simultaneously the time was recorded with the help of stop watch to fill the specified volume of 5000 ml measuring beaker. Calibration data for rotameter in given in Annexure Table A1, Figure 3.3 below shows the calibration graph.

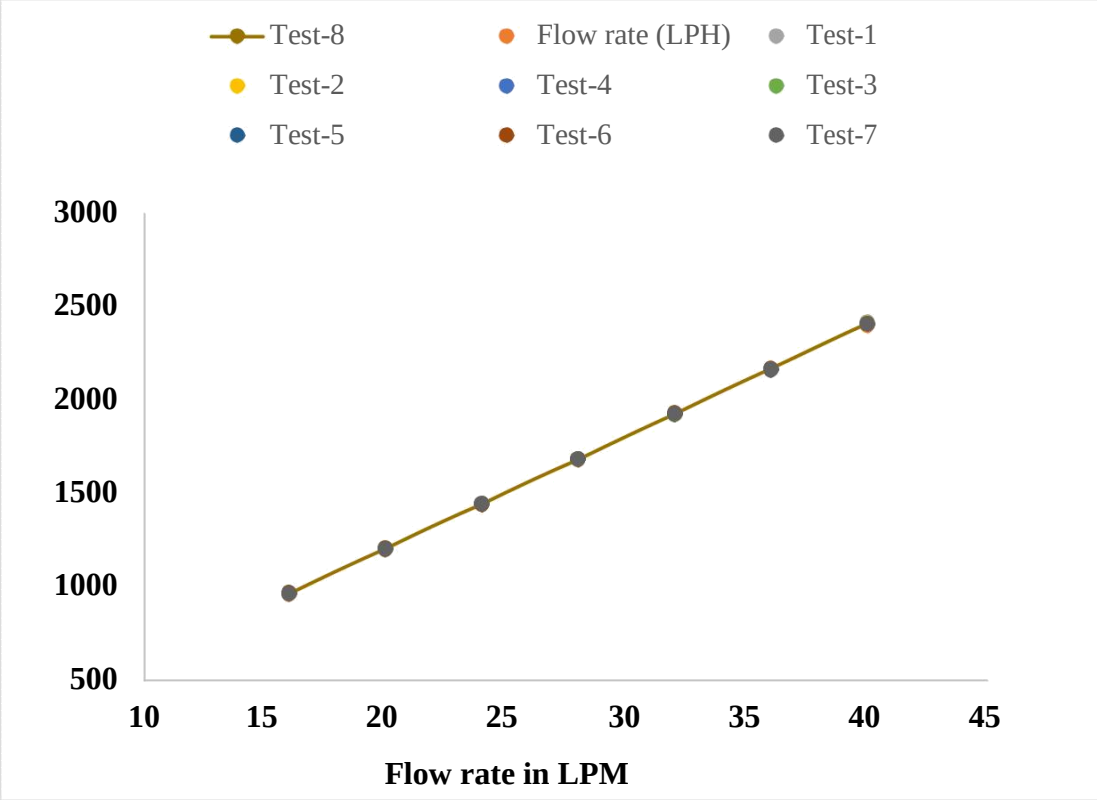

Figure 3.3: Rotameter calibration graph.

5. **Test section**: The setup consists test section of galvanized iron of 1524 mm long and 19 mm diameter pipe, well connected with flexible pipe. Flow through the pipe is controlled with the help by-pass valve connected just below the rotameter. The required flow rate is measured on the measuring scale of rotameter which is calibrated before performing the experiments. The master solution of different concentrations are injected in the test section with the help of peristaltic pump. The injection slots of 5 mm diameter are gas welded on the surface of the test section, it is shown in Figure 3.4.

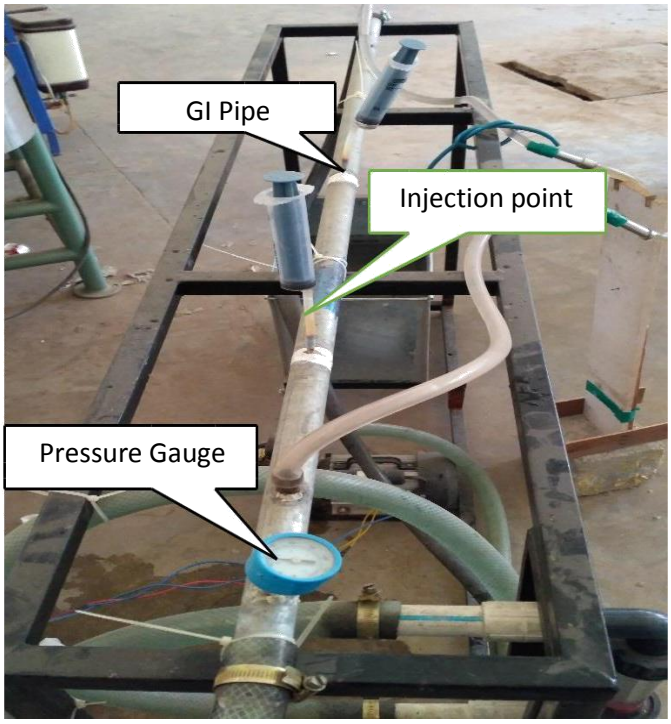

Figure 3.4: Photographic view of test section.

6. **U-tube manometer:** U-tube differential type manometer with mercury as manometric fluid is used in the experiment to measure the pressure drop across the pipe in the test section. The manometric fluid, is decided on the basis of its density and immiscibility as compared to the fluid whose pressure gradient is to be measured. The two limbs are connected through tubes at the inlet and outlet of galvanized iron pipe in test section.

7. **Peristaltic pump:** The peristaltic pump is used to inject the master solution of different concentrations in the test-section. It is also known as tubing pump is a type of positive displacement pump. It features a unique design, a drive system that turns a set of rollers which compress and release the flexible tubing as they rotate. Now, this squeezing action creates the vacuum that draws fluid through the tubing. It is self-priming and non-siphoning, that can handle high viscosities and shear sensitive fluids.

3.4 Preparation of master solution

Preparation of master solution plays a vital role in this experimental study. A master solution of different concentrations is prepared by dissolving the appropriate amount of biopolymer, weighed by weight scale. It is then sprinkled in a beaker containing tap water while mixing with the paddle stirrer to form a homogenous solution. The speed of the stirrer is

controlled by the regulator at regular interval of 30 minutes between the ranges of 1500-2400 rpm.

3.5 Measurement of viscosity of polymer solution

Viscosity is the measure of friction or resistance of fluid to the flow. Brookfield viscometer of LV model with SC4-31 spindle is used to measure the viscosity of prepared polymer solutions with different concentrations. It has been observed that with the increase in shear strain, the viscosity decreases exhibiting the shear thinning property. The viscometer operates on the principle that spindle is driven by a calibrated spring that measures the viscous effect of the fluid on the spindle by the deflection of the spring, and this deflection is measured by the transducer All the measurements are done at ambient temperature of (25±0.5) ºC and compared with the power law.

3.6 Measurement of pH of polymer solutions

The pH of a solution expresses the acidic or alkalinity of the solution on logarithmic scale on which 7 being neutral and the values more than 7 are alkaline and lower values are acidic. The pH of all the polymer solutions with different concentrations, used in the experimentation is found. It is observed that for all concentrations of guar gum, the pH is less than 7 and for hydroxyethyl cellulose it is more than 7. The pH of GG and HEC at different concentrations is shown in Figure 3.5.

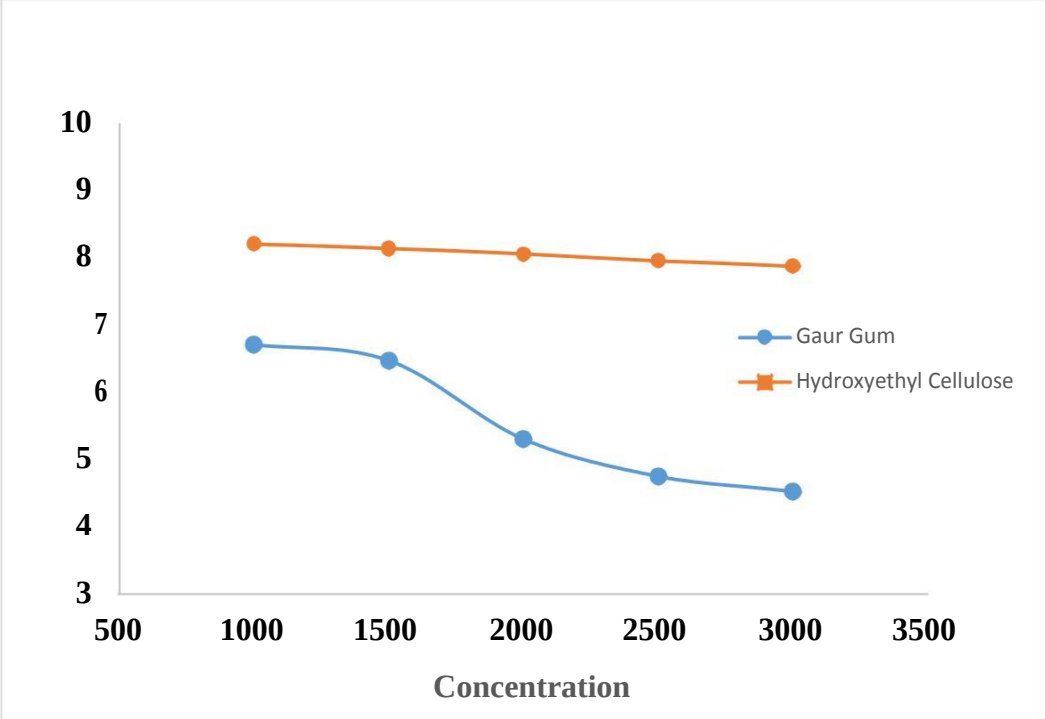

Figure 3.5: pH of GG and HEC at different concentrations.

3.7 Equations used in the study

The basic quantities measured in this experimental study are:

1. Reynold number (Re) the ration of inertial force by viscous force [9] is measured from the relation

   $Re = \rho V D_{\mu}$

   where,

   ρ = density of the fluid. V = velocity.

   D = diameter of the pipe.

   μ = dynamic viscosity.

2. Entrance length (L_e) defines the fully developed flow [37] is measured from the relation

   $L_e = 4.4*(\ )^{1/6}*D$

3. Velocity of the flow in the test section is measured by

$V = \frac{Q}{\pi r^2}$

where,

Q = discharge.

r = radius of the pipe.

4. The volume of water in the entire pipe section of experimental setup is calculated by

$v = \pi * r^2 * L$ where,

r = radius of the pipe.

L=length of the pipe.

5. The pressure drop [37] across the pipe (Δ) = g*(Δh)*($-$) where.

g = acceleration due to gravity.

Δh = change in mercury level from scale.

= density of mercury.

= density of water.

6. The mean shear stress near the wall (τ) for both Newtonian and Non-Newtonian fluids for all the flow regimes is measured from the relation [9]

$\tau = \frac{\Delta * \Delta}{4 * \Delta}$

where,
Δ = pressure drop across the pipe.
Δ = distance across which the pressure drop is calculated.

7. The friction factor(f) is calculated with respect to the wall shear stress [9]

$f = \frac{\tau}{\frac{1}{2} * \rho * v^2}$

8. The head losses [37] in the experimental setup is calculated from the following relation

   $h_L = f\frac{L}{D}\frac{V^2}{2g}$

   where,

   $\frac{L}{D}$ = length to diameter ratio.

   V = velocity.

9. Hydraulic Power of pump [37] is measured from the relation

   $h = \rho * g * Q * h_{3.6*106}$ kW

   where,

   Q = flow capacity in ( ).

10. Hydraulic Horse Power = $0.746\overline{h}$ hp.

Summary

All the basic quantities used in this experimental study are discussed in this chapter. The rotameter used in the setup for measuring the flow rate is properly calibrated. The pH of all the polymer solutions with different concentrations, used in this experimentation is also found which defines the acidic or alkalinity nature of all the polymer solutions.

CHAPTER 4
Results and Discussion

The variation of drag reduction rate with respect to different parametric conditions are discussed in this chapter.

4.1 Reduction of friction factor with polymer solution

From the experimental study of Virk [38], the polymer solution and water shows similar behavior in the laminar region and also for the turbulent flow for the range of 3000 < Re < 12000, polymer solution results are identical as solvent. It was found that onset of drag reduction is witnessed for Reynolds number greater than 12000, the polymer solution data diverges from the solvent towards the lower friction. It was also observed that drag reduction rate increases significantly with increase in the flow rate of polymer solution. It is evident that specific energy required to maintain turbulent flow of the polymer solution can be significantly less than that compared to solvent alone.

The gross flow studies involve measurements of pressure drop against the flow rate in the test section, which introduces the phenomenon of drag reduction. The results shown in Figure 4.1 and Figure 4.2 are obtained in the same pipe of the test section for solvent and polymer solutions of different concentration for guar gum and hydroxyethyl cellulose. The data is plotted in two ways Figure 4.1 and Figure 4.2, shows the data of non-dimensional coordinates of fanning friction factor and Reynolds number. In this it is observed that with increasing Reynolds number the friction factor approaches close to zero for the polymer solution.

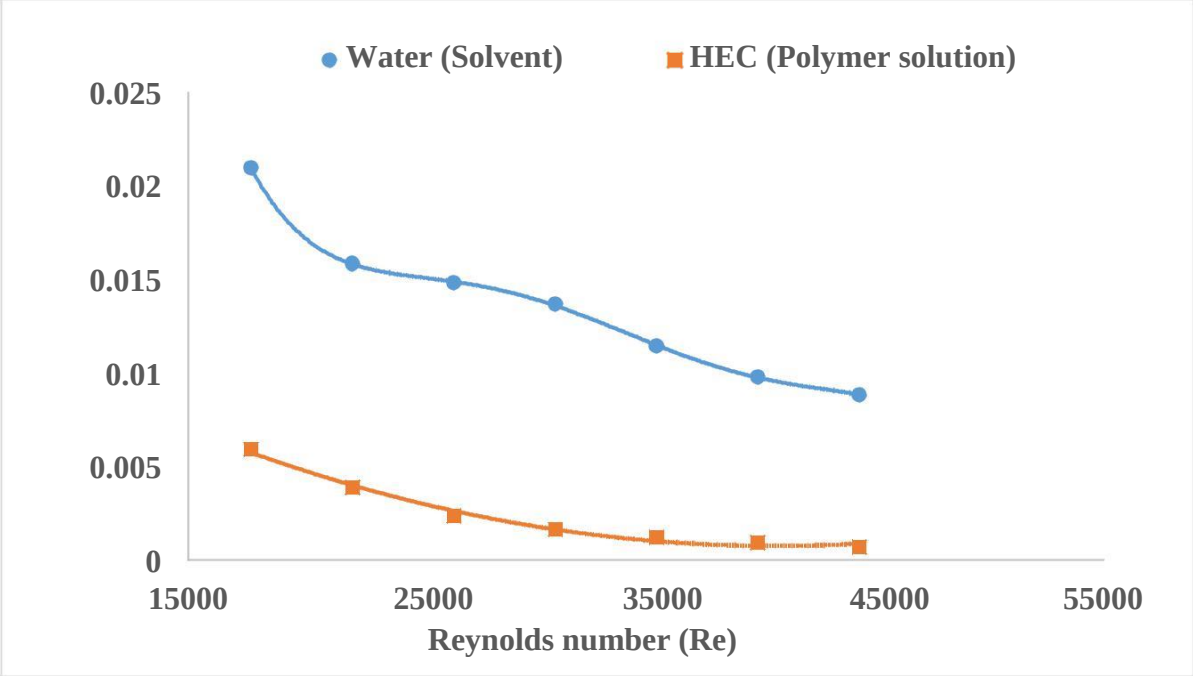

Figure 4.1: Non-dimensional friction factor and reynolds number for hydroxyethyl cellulose.

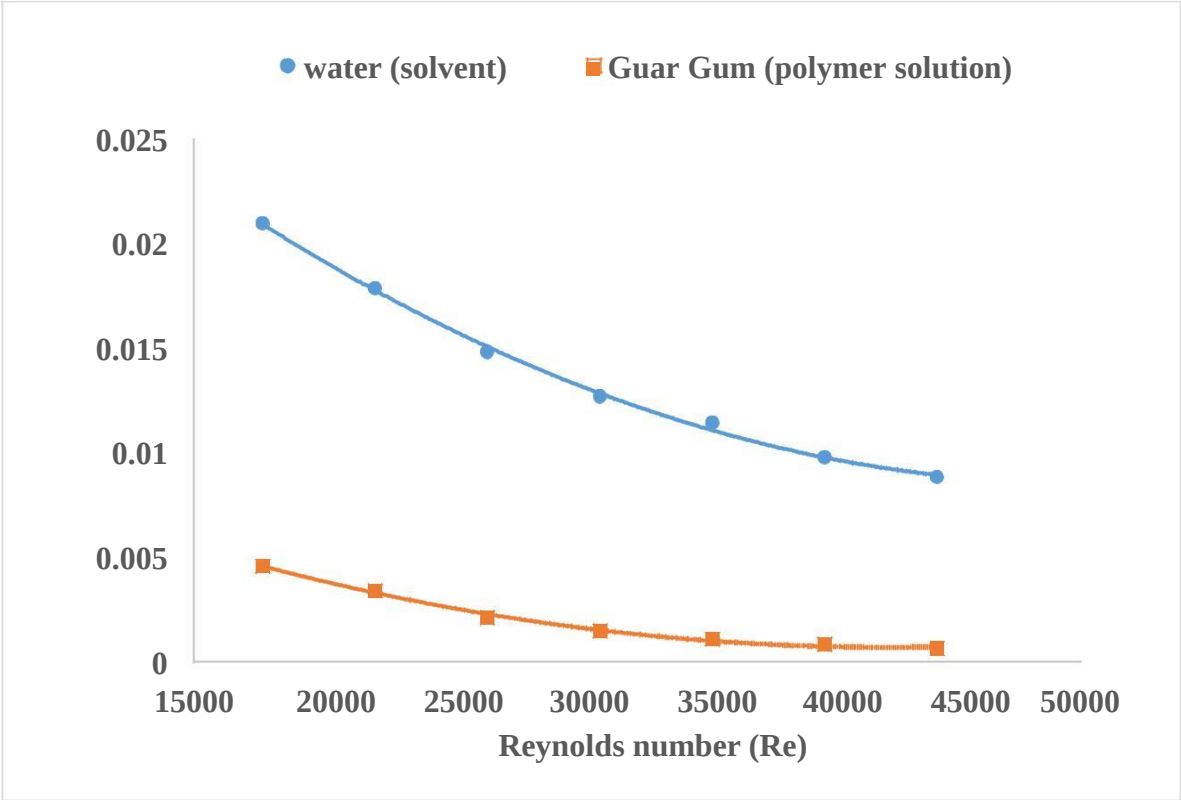

Figure 4.2: Non-dimensional friction factor and reynolds number for guar gum.

While Figure 4.3 and Figure 4.4 shows the Prandtl-von Karman form of plotting 1/√ and Re√ for guar gum (GG) and hydroxyethyl cellulose (HEC).

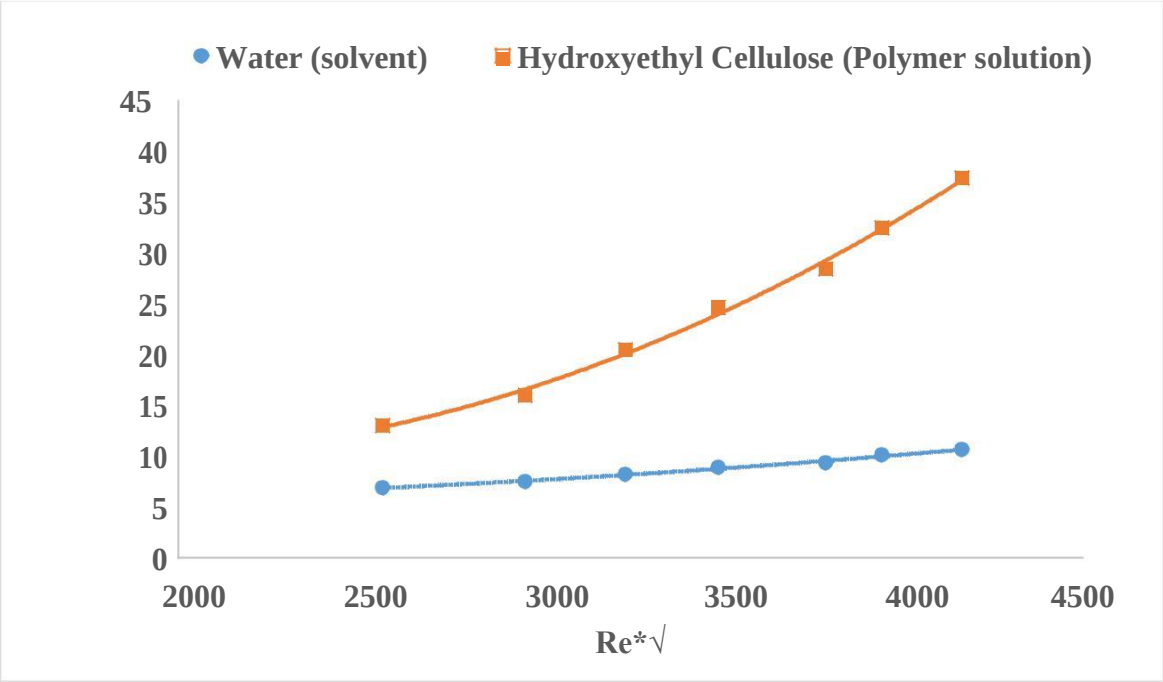

Figure 4.3: Prandtl-von karman form of plotting for hydroxyethyl cellulose.

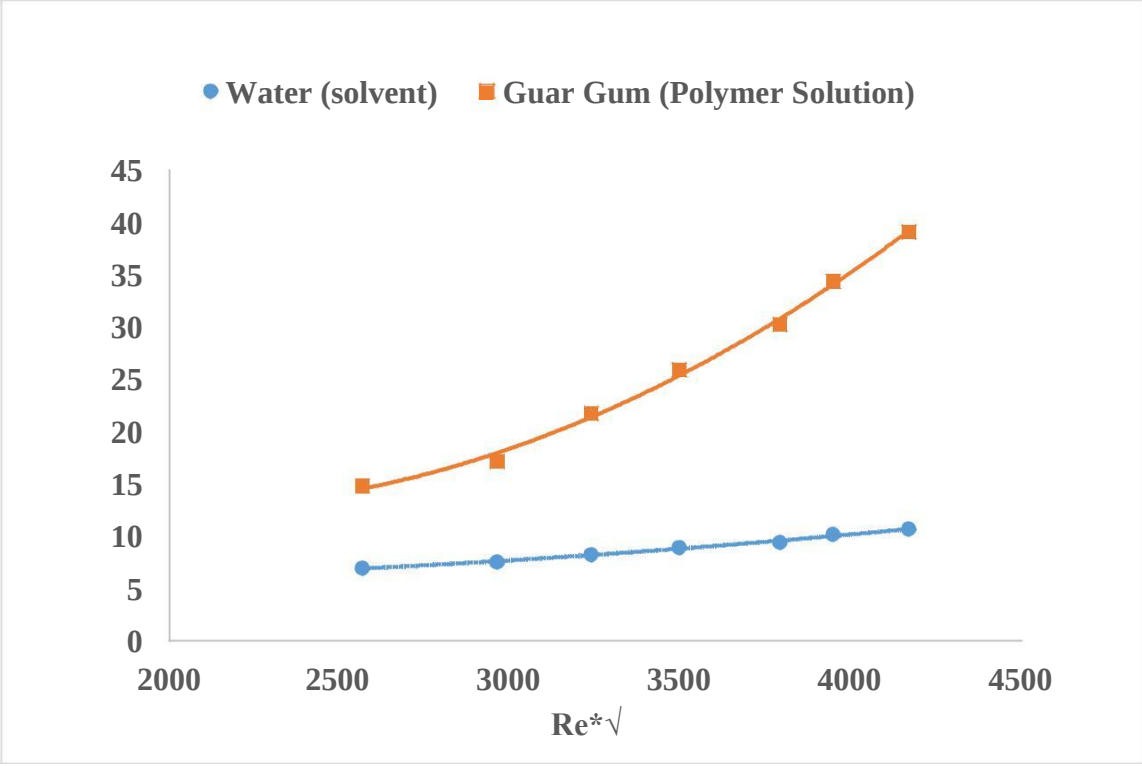

Figure 4.4: Prandtl-von karman form of plotting for guar gum.

In this study, the flow behavior at Reynolds number greater than 17000 and mechanical degradation due to the centrifugal pump have been studied. The percentage of drag reduction (%DR) is calculated using the following relation [9]:

$$\%DR = \frac{\Delta P_{\text{without DRP}} - \Delta P_{\text{with DRP}}}{\Delta P_{\text{without DRP}}} \quad (4.1)$$

The results obtained from the experimental study are given in the Table 4.1 and 4.2:

Table 4.1: Drag reduction percentage at different Reynolds number and concentrations for guar gum.

Reynolds number	**%DR (3000 ppm)**	**%DR (2500 ppm)**	**%DR (2000 ppm)**	**%DR (1500 ppm)**	**%DR (1000 ppm)**
17723.891	42.343	37.050	31.757	28.582	25.406
22154.864	50.042	46.289	43.787	38.783	35.029
26585.837	58.944	53.892	50.523	45.471	42.103
31016.809	67.75	63.515	59.281	53.988	50.812
35447.782	71.599	66.98	62.36	56.586	53.122
39878.755	72.562	70.059	67.557	62.553	57.549
44309.728	75.352	72.562	69.771	64.747	60.003

Table 4.2: Drag reduction percentage at different Reynolds number and concentrations for hydroxyethyl cellulose.

Reynolds number	**%DR (3000 ppm)**	**%DR (2500 ppm)**	**%DR (2000 ppm)**	**%DR (1500 ppm)**	**%DR (1000 ppm)**
17723.891	47.636	43.402	38.109	35.992	32.816
22154.864	56.298	51.418	46.289	43.787	40.034
26585.837	65.681	58.102	55.576	51.029	47.324
31016.809	69.867	65.633	61.398	58.222	56.105
35447.782	73.909	68.828	64.901	62.36	60.051
39878.755	75.064	72.562	68.558	65.055	63.053
44309.728	77.585	74.236	71.166	67.259	65.584

High molecular weight guar gum and hydroxyethyl cellulose at different concentrations and Reynolds number, taken as parameters of study to observe the influence of biopolymers in drag reduction. High molecular weight polymers are more likely to be able to interact with

bigger vortices and responsible for higher percentage of drag reduction [45]. From the experimental study it is observed that maximum percentage of drag reduction is achieved at high concentrations and at high Reynolds number.

4.2 Effect of concentration in drag reduction

Figure 4.5 and 4.6 shows the dependence of concentration on percentage of drag reduction. It shows that drag reduction depends on the flow rates, which is directly proportional to Reynolds number. With increase in concentration of polymer solutions hydroxyethyl cellulose (HEC) exhibits more percentage of drag reduction around 77.5% as compared to 75.3% by guar gum at 3000 ppm and at 1000 ppm we observe 65.5% by HEC and 60% by GG. The drag reduction percentage increases gradually for varying concentrations between 1000 ppm to 3000 ppm.

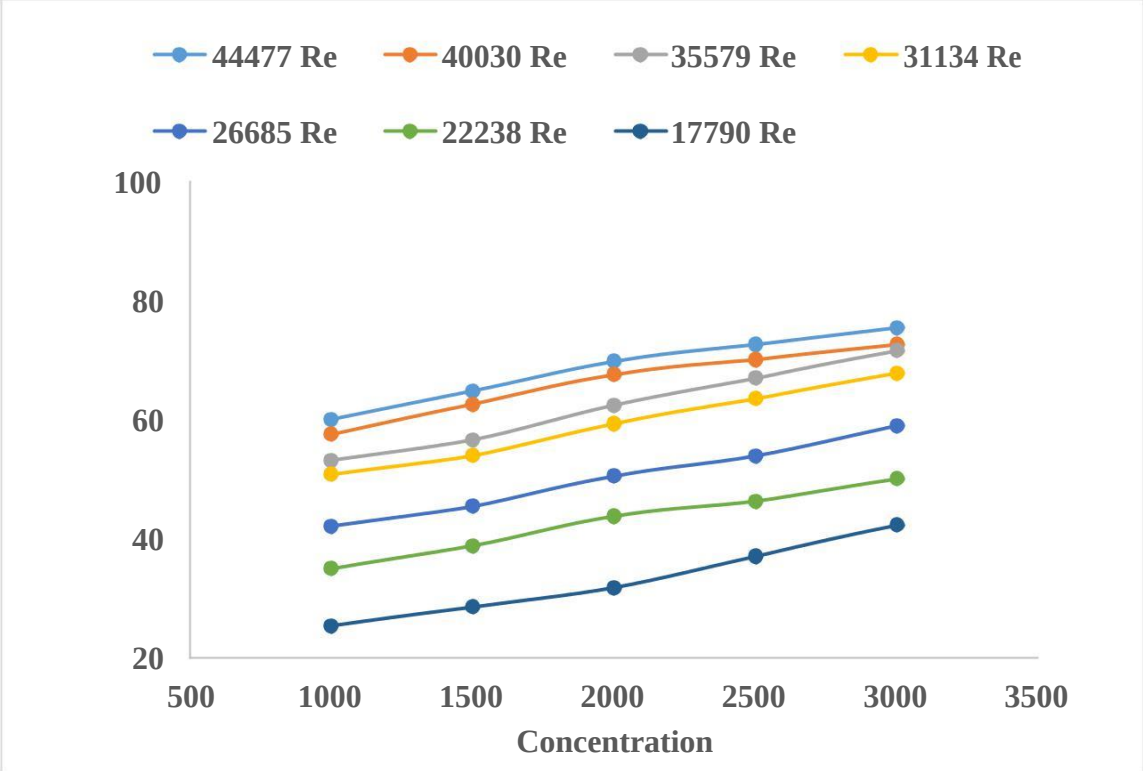

Figure 4.5: Effect of concentration on percentage of drag reduction for guar gum.

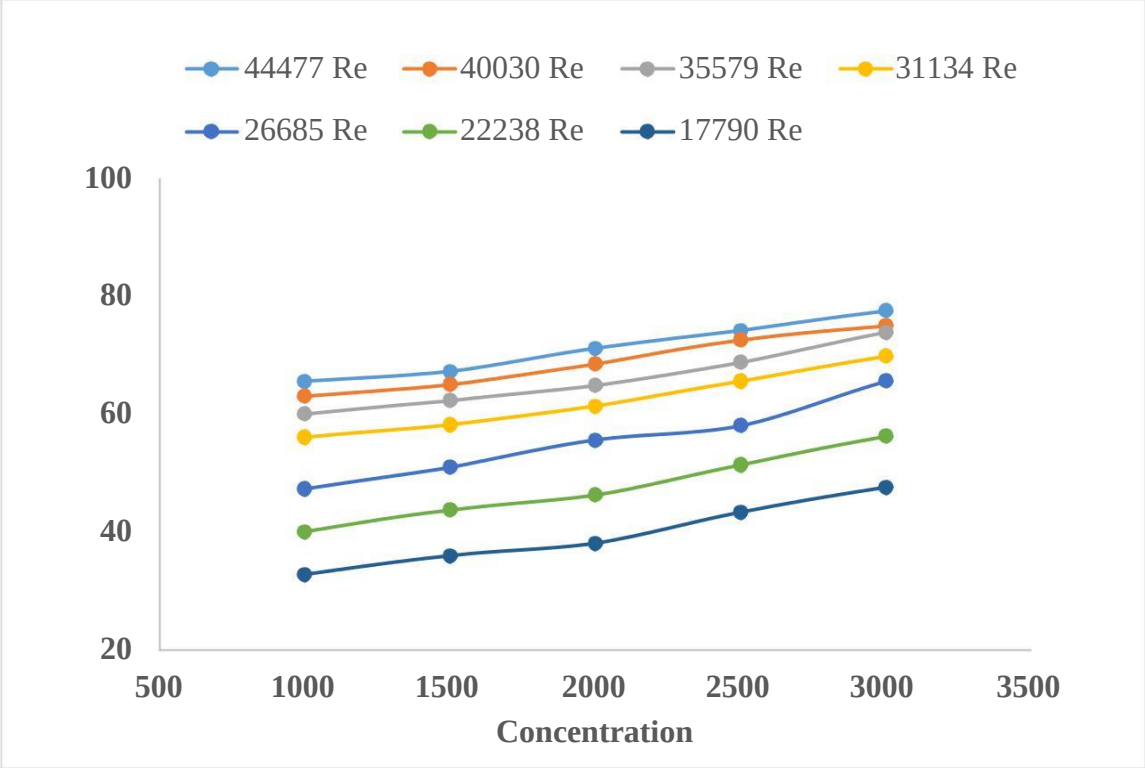

Figure 4.6: Effect of concentration on percentage of drag reduction for hydroxyethyl cellulose.

4.3 Effect of Reynolds number and concentration in drag reduction

Figure 4.7 and 4.8 shows the drag reduction dependence on Reynolds number at different concentrations for guar gum and hydroxyethyl cellulose. Even at constant Reynolds number, the drag reduction percentage varies with the concentrations. The percentage of drag reduction is found to be 42.34 % for guar gum and 47.63% for hydroxyethyl cellulose at Reynolds number of 17723. The drag reduction percentage increases with the Reynolds number in the pipe section for both the biopolymers. The maximum percentage of drag reduction is found at Reynolds number of 44000 with 3000 ppm, and lowest percentage of drag reduction is found at Reynolds number of 17723 with 1000 ppm for both the polymers.

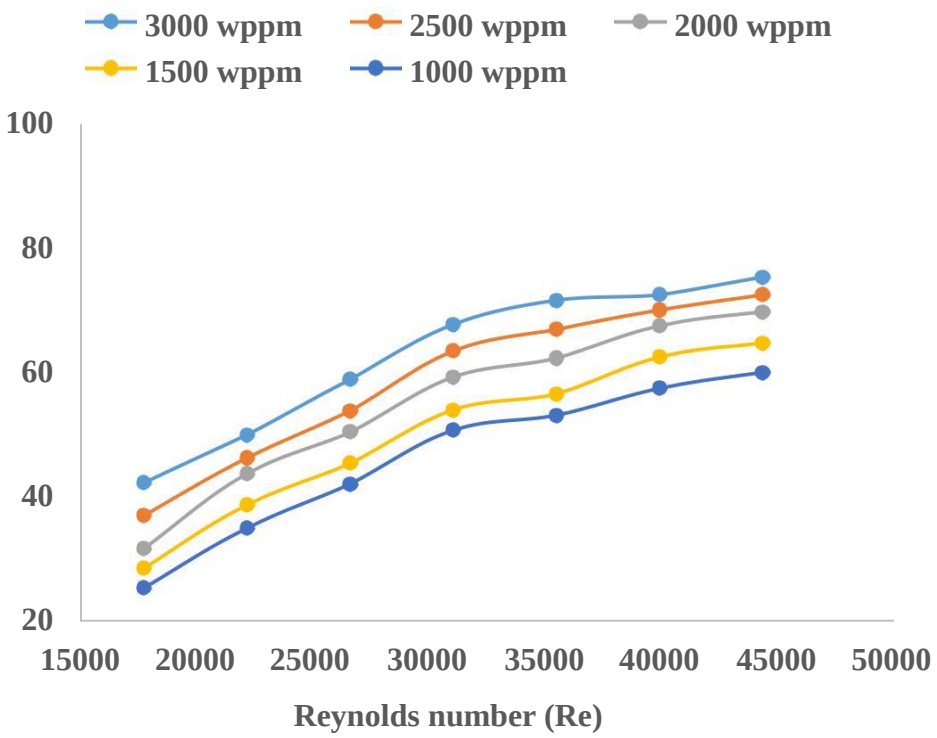

Figure 4.7: Drag reduction dependence on Reynolds number at different concentrations for guar gum.

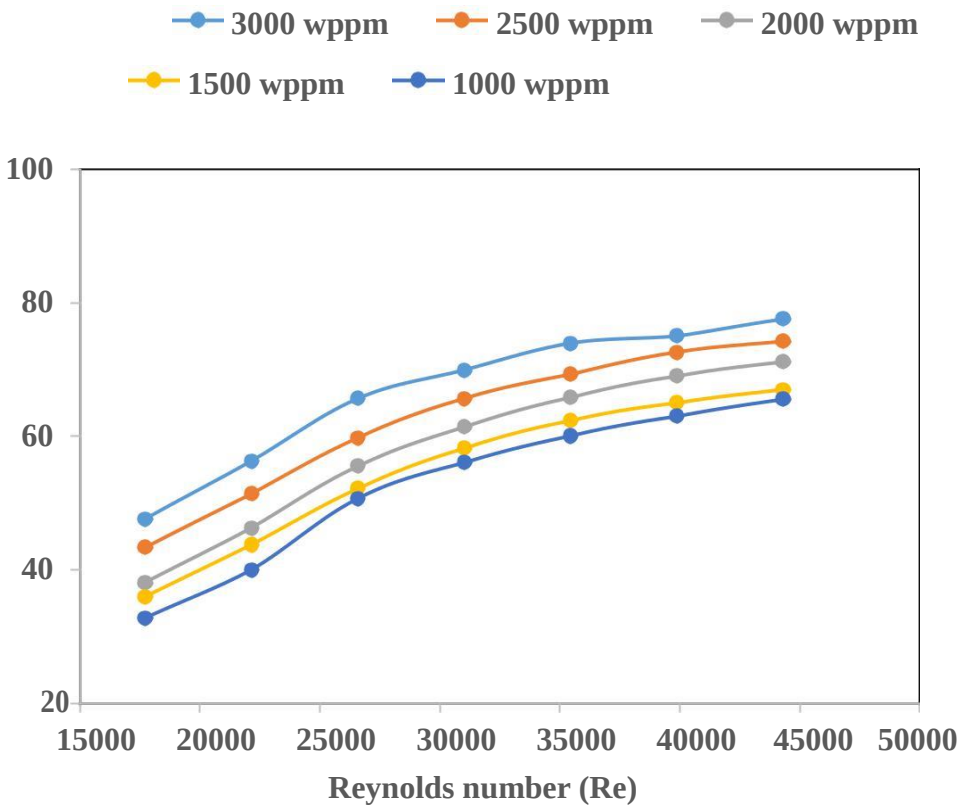

Figure 4.8: Drag reduction dependence on Reynolds number at different concentrations for hydroxyethyl cellulose.

In fully developed turbulent pipe flow, dilute polymer solutions exhibits three different regimes in order of increasing flow rates [4].

1. Without drag reduction in which the fanning friction factor relation is similar for solvent, usually Prandtl-von Karman law for Newtonian turbulent pipe flow:

$$^{-1/2} = 4.0\log_{10}(Ref^{1/2}) - 0.4 \quad (4.2)$$

2. With drag reduction in which friction factor relation depends on the nature of polymer solution. An approximate relation for this regime:

$$^{-1/2} = (4.0+\delta)\log_{10}(Ref^{1/2}) - 0.4 - \delta\log_{10}\sqrt{2}dW^{n} \quad (4.3)$$

where d and W^{o} are polymer solution parameters.

3. A regime of maximum drag reduction asymptote in which friction factor relation is insensitive to polymer solution employed universally:

$$^{-1/2} = 19.0\log_{10}(Ref^{1/2}) - 32.4 \quad (4.4)$$

4.4 Comparison between polymer solution and von-Karman asymptote

Figure. 4.9 and 4.10 illustrates the deviation of polymer solutions of different concentrations from the Prandtl-von Karman asymptote. This deviation is due to the Non-Newtonian behavior of the polymer solution. The tap water used as solvent in the experiment shows the Newtonian behavior as it close to the Prandtl-von Karman asymptote. In this study it is found that pressure drop across the test section depends on the concentration of polymer solution and so does the friction factor. It is observed that high concentration polymer solutions are more effective in drag reduction at higher Reynolds number. From the experimental results, the deviation of hydroxyethyl cellulose and gaur gum from Prandtl von-Karman equation is given by the following relations:

For hydroxyethyl cellulose,

$$(f)^{-1.66395} = 1.86\times10^{-7}(Re)^{2.3279} + B \quad (4.5)$$

For guar gum,

$$(f)^{-1.58939} = 5.4\times10^{-7}(Re)^{2.17878} + C \qquad (4.6)$$

The difference between the values of van-Karman asymptote and results obtained for different concentrations are denoted by constants B and C in the above equations. The values of B varies from 1.24 at Reynolds number of 17723 to 23.7 at Reynolds number of 44309 for 1000 ppm for hydroxyethyl cellulose. The values of B and C varies significantly with different polymer concentrations. The values of C varies from 2.5 at Reynolds number of 17723 to 25.399 at Reynolds number of 44309 for 1000 ppm of guar gum.

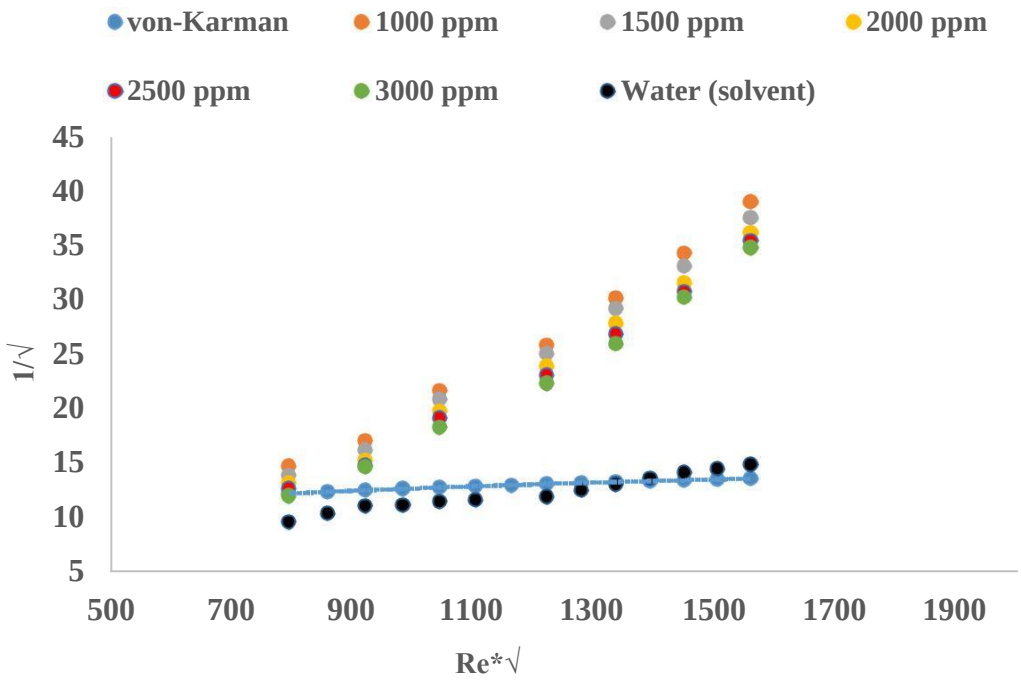

Figure 4.9: Comparison of prandtl-von karman asymptote with water and guar gum with different concentrations.

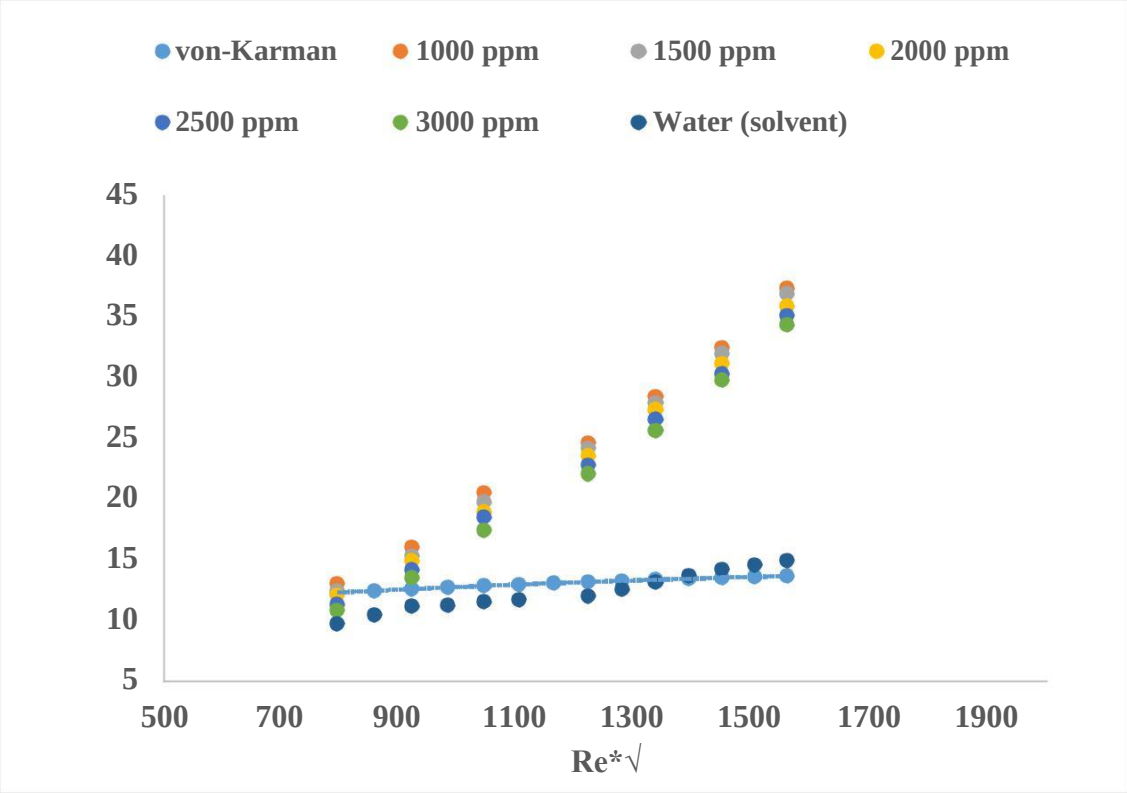

Figure 4.10: Comparison of prandtl-von karman asymptote with water and hydroxyethyl cellulose with different concentrations.

4.5 Validation of drag reduction with MDR asymptote

Percentage of maximum drag reduction that can be achieved is limited to the unique asymptote illustrated in Figure 4.11 and Figure 4.12. It is also found that percentage of drag reduction exceeds maximum drag reduction (MDR) asymptote for Reynolds number greater than 35000. The drag reduction rate exceeds by maximum of 23.28% for guar gum and 21.5% for hydroxyethyl cellulose at Reynolds number of 44300 for 3000 ppm polymer concentration. For the flows with Reynolds number less than 35000, the drag reduction rate is within the limits.

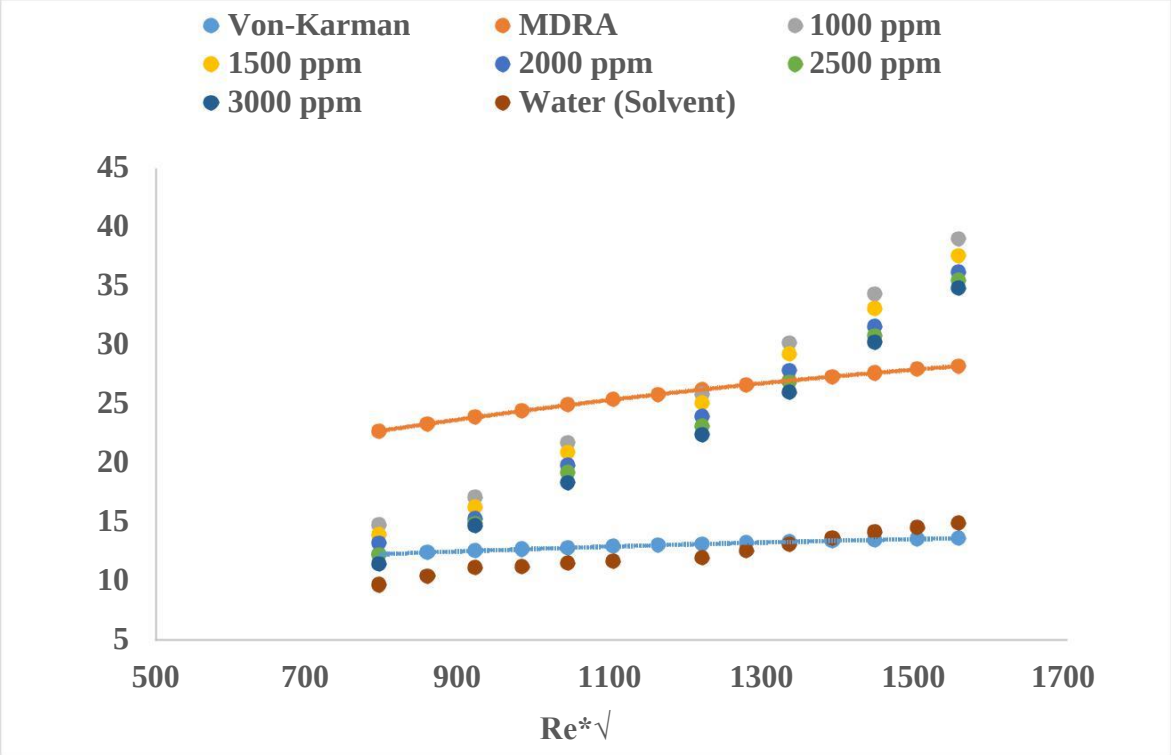

Figure 4.11: Validation of drag reduction with Prandtl-von Karman and maximum drag reduction (MDR) asymptotes for guar gum with different concentrations.

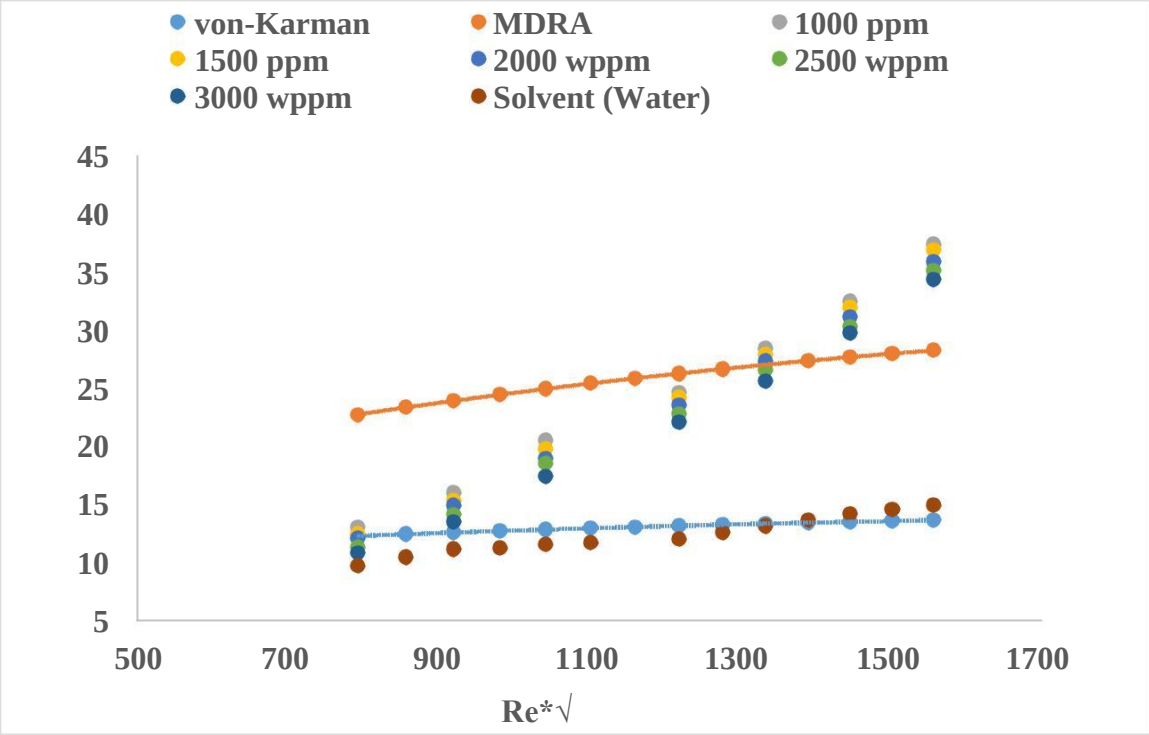

Figure 4.12: Validation of drag reduction with Prandtl-von Karman and maximum drag reduction (MDR) assymptotes for hydroxyethyl cellolose with different concentrations.

4.6 Polymer degradation

An important problem in the study and application of drag reduction by polymer additives is the degradation of polymers. Drag reduction capability of polymer is limited to two types of degradation: mechanical and chemical [28].

Chemical degradation occurs when the polymer structure changes due to chemical reaction. It can be caused due to the presence of metals where oxygen is present and high level of salinity or calcium in solvent can also cause chemical degradation [41].

Mechanical degradation is the process of rupture of polymer molecules into smaller aggregates occurs due to mechanical forces acting on the polymers, when the fluid passes through pump or pipe or both. The mechanical stress causes the polymers to break and thus reduces the molecular weight which reduces the drag reducing capability. Practical use of polymers in turbulent drag reduction application is mostly hindered by mechanical degradation.

In this study, it is also found that drag reducing polymers (DRP's) loses their effectiveness when subjected to longer run time under identical run conditions. The structures of biopolymers are more rigid than the synthetic polymers, they show better shear stability [42, 43]. Due to high shear stability of polymer molecules do not break with immediate effect. In Figure 4.13 the mechanical degradation of guar gum at different Reynolds number or flow rates are shown. It is observed that degradation time for guar gum depends on Reynolds number at a particular concentration. Complete degradation for guar gum at 3000 ppm takes approximately 42 minutes at Reynolds number of 44000.

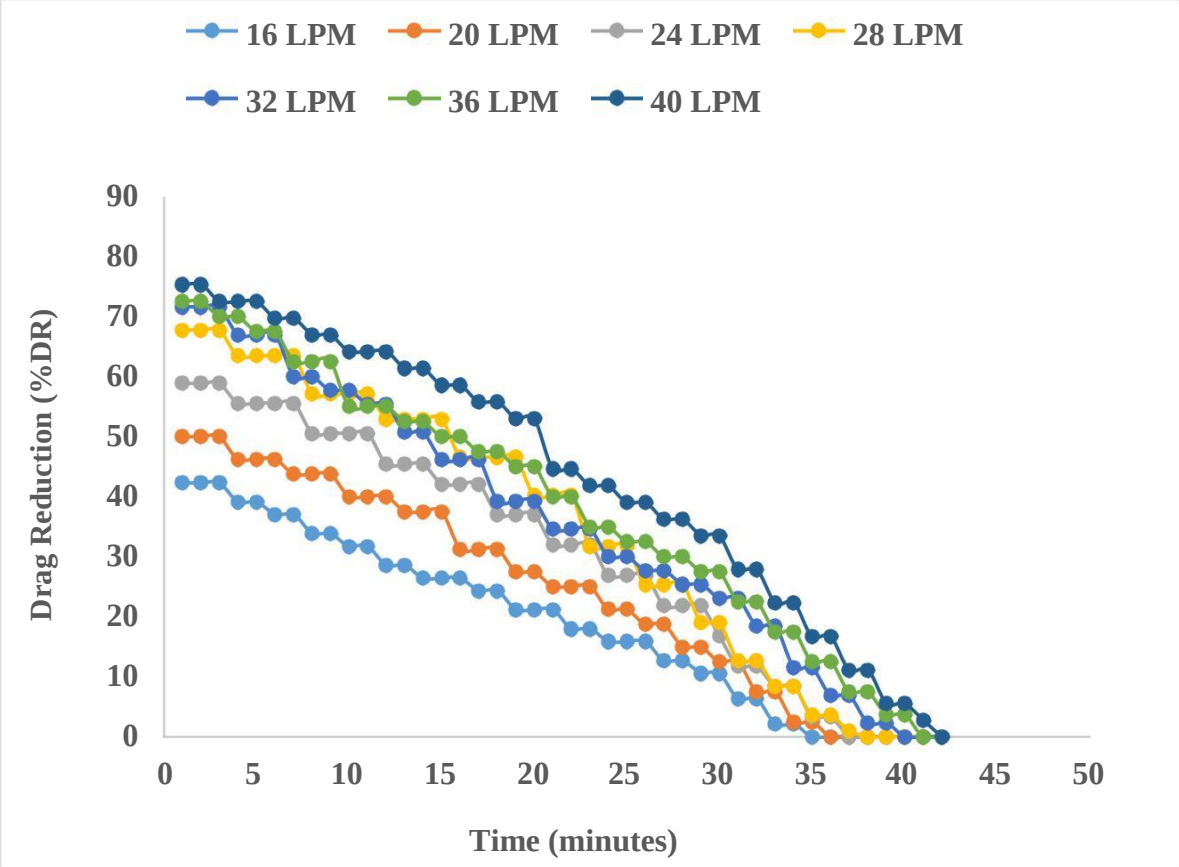

Figure 4.13: Reduction of %DR with time for 3000 ppm concentration of guar gum.

Hydroxyethyl cellulose shows better resistance to the mechanical degradation than guar gum. The mechanical degradation is observed due to the centrifugal pump, when the same water is recirculated through the test-section i.e., same polymer solution recirculates through the test section. Complete degradation of HEC at 3000 ppm takes approximately 46 minutes at Reynolds number of 44000.

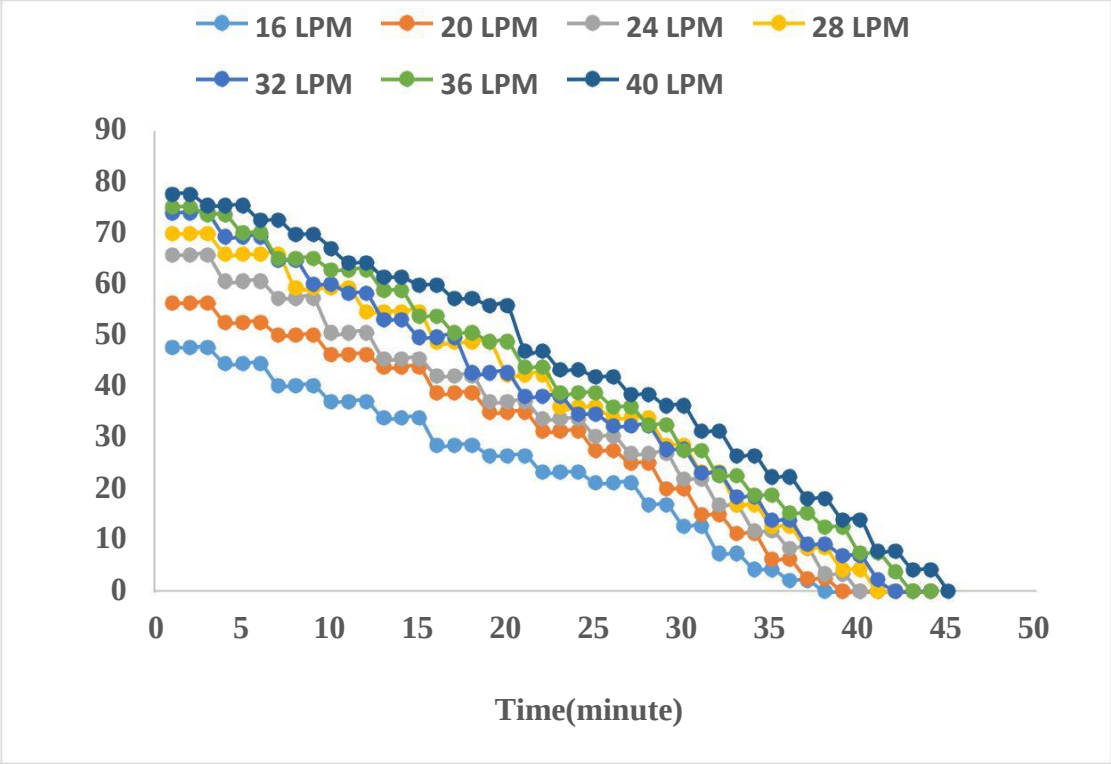

Figure 4.14: Reduction of %DR with time for 3000 ppm concentration of hydroxyethyl cellulose.

From the results, it is found that hydroxyethyl cellulose (HEC) shows better sustainability to mechanical degradation than guar gum (GG) under identical operating conditions.

Chapter-5
Conclusion and Future Scope

5.1 Conclusion

Experimental study has been performed in a single phase water flow in a pipe. In this experimental study effect of polymer solutions with different concentrations on skin friction drag were examined at different Reynolds numbers. Five different concentrations of guar gum and hydroxyethyl cellulose are used in this experimental study and each solution is injected in the pipe of test-section at different Reynolds number. By injecting the polymer solution in the test section there is a significant change in the pressure drop across the test-section. From this percentage of drag reduction can be measured for each concentration at different Reynolds number. The conclusion drawn from this experimental study is:

1. With increase in concentration of polymer solutions, percentage of drag reduction increases significantly. Hydroxyethyl cellulose (HEC) exhibits more percentage of drag reduction around 77.5% as compared to 75.3% by guar gum at 3000 ppm. The drag reduction percentage increases gradually by varying the concentrations between 1000 ppm to 3000 ppm.
2. Even at constant Reynolds number, the drag reduction percentage varies with the concentrations. The percentage of drag reduction is found to be 42.34 % for guar gum and 47.63% for hydroxyethyl cellulose at Reynolds number of 17723. The drag reduction percentage increases with the Reynolds number in the pipe section for both the biopolymers. The maximum percentage of drag reduction is found at Reynolds number of 44000 with 3000 ppm, and lowest percentage of drag reduction at Reynolds number of 17723 with 1000 ppm for both the polymers.
3. Hydroxyethyl cellulose shows better resistance to the mechanical degradation than guar gum. The mechanical degradation is observed due to the centrifugal pump, when the same water is recirculated through the test-section for a run time of 30 minutes. Complete degradation of HEC at 3000 ppm takes approximately 46 minutes while guar gum takes at Reynolds number of 44000.

4. Hence, hydroxyethyl cellulose (HEC) is found to be a better drag reducing polymer than guar gum (GG).

5.2 Future Scope

The phenomenon of polymer induced drag reduction in a turbulent flow has drawn lot of attention ever since its discovery in 1949. Modification of turbulence with polymer additives is a broad undiscovered area. Despite wide range of numerical analysis and experimental work, exact mechanism behind this phenomenon still remains unknown. Hence more research should be done on the following basis.

1. Effect of drag reducing fibres in homogenous mixture of biopolymer could increase the shear durability of polymers since fibres are mechanically more stable which can also result in increased drag reduction rate.
2. Effect of temperature on drag reduction rate in presence of biopolymers should be investigated for enhancing the range of practical applications.
3. By using the Laser Doppler Anemometer to study the velocity profile can give better insight into the mechanism of drag reduction.
4. Research can be done on recovering and reusing the biopolymers from the working fluid that may reduce the cost of the entire process.

References

1. Lester, C. B. (1985). The basics of drag reduction. Oil Gas J. (United States), 83(5).
2. Kulmatova, D., Turbulent drag reduction by additives, PhD Thesis, University of Amsterdam, 2013. (http://dare.uva.nl/search?metis.record.id=398395)
3. Mahmoud, N. M., Physico-chemical study on guar gum, Master Thesis, University of Khartoum,Sudan,2000. (http://www.iaea.org/inis/collection/NCLCollectionStore/_Public/32/042/32042657. pdf)
4. Virk, P. S., Drag reduction fundamentals, AIChE Journal, vol. 21, no. 4, pp. 625–656, 1975.
5. Bewersdorff, H. W., & Berman, N. S. (1988). The influence of flow-induced non-Newtonian fluid properties on turbulent drag reduction. Rheologica Acta, 27(2), 130-136.
6. Warholic, M. D., Massah, H., and Hanratty, T. J., Influence of drag-reducing polymers on turbulence: effects of Reynolds number, concentration and mixing, Experiments in Fluids, vol.27, no. 5, pp. 461–472, 1999.
7. Lumley, J. L. (1969). Drag reduction by additives. Annual review of fluid mechanics, 1(1), 367-384.
8. Min, T., Choi, H., & Yoo, J. Y. (2003). Maximum drag reduction in a turbulent channel flow by polymer additives. Journal of Fluid Mechanics, 492, 91-100.
9. Ptasinski, P. K., Boersma, B. J., Nieuwstadt, F. T. M., Hulsen, M. A., Van den Brule, B. H. A. A., & Hunt, J. C. R. (2003). Turbulent channel flow near maximum drag reduction: simulations, experiments and mechanisms. Journal of Fluid Mechanics, 490, 251-291.
10. Li, C. F., Sureshkumar, R., & Khomami, B. (2006). Influence of rheological parameters on polymer induced turbulent drag reduction. Journal of Non-Newtonian Fluid Mechanics, 140(1), 23-40.
11. Burger, E. D., Munk, W. R., & Wahl, H. A. (1982). Flow increase in the Trans Alaska Pipeline through use of a polymeric drag-reducing additive. Journal of Petroleum Technology, 34(02), 377-386.
12. Berge, B. K., & Solsvik, O. (1996, January). Increased pipeline throughput using drag reducer additives (DRA): Field experiences. In European Petroleum Conference. Society of Petroleum Engineers.
13. Jacobs, B. E. (2003). Design of slurry transport systems. Crc Press.

14. Eichenberger, H. P. (1962). U.S. Patent No. 3,016,865. Washington, DC: U.S. Patent and Trademark Office.
15. Marhefka, J. N., Marascalco, P. J., Chapman, T. M., Russell, A. J., & Kameneva, M. V. (2006). Poly (N-vinylformamide) A Drag-Reducing Polymer for Biomedical Applications. Biomacromolecules, 7(5), 1597-1603.
16. Gasljevic, K., & Matthys, E. F. (1993). On saving pumping power in hydronic thermal distribution systems through the use of drag-reducing additives. Energy and Buildings, 20(1), 45-56.
17. Inaba, H., Inada, T., Horibe, A., Suzuki, H., & Usui, H. (2005). Preventing agglomeration and growth of ice particles in water with suitable additives. International Journal of Refrigeration, 28(1), 20-26.
18. Lumley, J. L. (1977). Drag reduction in two phase and polymer flows. The Physics of Fluids, 20.10, S64-S71.
19. Hinch, E. J. (1977). Mechanical models of dilute polymer solutions in strong flows. The Physics of Fluids, 20(10), S22-S30.
20. Landahl, M. T. (1973). Drag reduction by polymer addition. In Theoretical and Applied Mechanics (pp. 177-199). Springer Berlin Heidelberg.
21. Ryskin, G. (1987). Turbulent drag reduction by polymers: a quantitative theory. Physical review letters, 59(18), 2059.
22. De Gennes, P. G. (1986). Towards a scaling theory of drag reduction. Physica A: Statistical Mechanics and its Applications, 140(1-2), 9-25.
23. Gyr, A., & Bewersdorff, H. W. (2013). Drag reduction of turbulent flows by additives (Vol. 32). Springer Science & Business Media.
24. Virk, P. S., Merrill, E. W., Mickley, H. S., Smith, K. A., & Mollo-Christensen, E. L. (1967). The Toms phenomenon: turbulent pipe flow of dilute polymer solutions. Journal of Fluid Mechanics, 30(02), 305-328.
25. Kim K., Li, C. F., Sureshkumar, R., Balachandar, S., & Adrian, R. J. (2007). Effects of polymer stresses on eddy structures in drag-reduced turbulent channel flow. Journal of Fluid Mechanics, 584, 281
26. Abubakar, A., Al-Hashmi, A. R., Al-Wahaibi, T., Al-Wahaibi, Y., Al-Ajmi, A., & Eshrati, M. (2014). Parameters of drag reducing polymers and drag reduction performance in single-phase water flow. Advances in Mechanical Engineering, 6, 202073.

27. Dubief, Y., White, C. M., Terrapon, V. E., Shaqfeh, E. S., Moin, P., & Lele, S. K. (2004). On the coherent drag-reducing and turbulence-enhancing behaviour of polymers in wall flows. Journal of Fluid Mechanics, 514, 271-280.
28. Den Toonder, J. M. J., Hulsen, M. A., Kuiken, G. D. C., & Nieuwstadt, F. T. M. (1997). Drag reduction by polymer additives in a turbulent pipe flow: numerical and laboratory experiments. Journal of Fluid Mechanics, 337, 193-231.
29. Graham, M. D. (2004). Drag reduction in turbulent flow of polymer solutions. Rheology reviews, 2, 143-170.
30. Bark, F. H., Hinch, E. J., & Landahl, M. T. (1975). Drag reduction in turbulent flow due to additives: a report on Euromech 52. Journal of Fluid Mechanics, 68(01), 129-138.
31. Ali, Q.M.A., and Talal A. Al-ausi, Drag Force Reduction of Flowing Crude Oil by Polymers Addition, the Iraqi Journal For Mechanical And Material Engineering, Vol.8, No.2, 2008
32. Kim, K., Adrian, R. J., Balachandar, S., & Sureshkumar, R. (2008). Dynamics of hairpin vortices and polymer-induced turbulent drag reduction. Physical review letters, 100(13), 134504.
33. Tian, M., Fang, B., Jin, L., Lu, Y., Qiu, X., Jin, H., & Li, K. (2015). Rheological and drag reduction properties of hydroxypropyl xanthan gum solutions. Chinese Journal of Chemical Engineering, 23(9), 1440-1446.
34. Terrapon, V. E., Dubief, Y., Moin, P., Shaqfeh, E. S., & Lele, S. K. (2004). Simulated polymer stretch in a turbulent flow using Brownian dynamics. Journal of Fluid Mechanics, 504, 61-71.
35. Petrie, H. L., Deutsch, S., Brungart, T. A., & Fontaine, A. A. (2003). Polymer drag reduction with surface roughness in flat-plate turbulent boundary layer flow. Experiments in Fluids, 35(1), 8-23.
36. Shoeibi Omrani, P., Delfos, R., & Boersma, B. J. (2012). Polymer Induced Drag Reduction in a Turbulent Pipe Flow Subjected to a Coriolis force. Flow, turbulence and combustion, 1-11.
37. Modi, P. N. & Seth, S. M. "Hydraulics and Fluid Mechanics Including Machine" (In SI Unit), new edition 2005-2006, Standard Book House.
38. Virk, P. S. (1971). Drag reduction in rough pipes. Journal of fluid mechanics, 45(02), 225-246.
39. Holland FA, Bragg R. Fluid flow for chemical engineers. 2nd ed. UK: Edward Arnold; 1995.

40. Khadom, A. A., & Abdul-Hadi, A. A. (2014). Performance of polyacrylamide as drag reduction polymer of crude petroleum flow. Ain Shams Engineering Journal, 5(3), 861-865.
41. Choi, K. S. (2001). Turbulent drag-reduction mechanisms: strategies for turbulence management. In Turbulence Structure and Modulation (pp. 161-212). Springer Vienna.
42. Singh, R. P. (1995). Advanced turbulent drag reducing and flocculating materials based on polysaccharides. In Polymers and other advanced materials (pp. 227-249). Springer US.
43. Melo, L. F., & Vieira, M. J. (1999). Physical stability and biological activity of biofilms under turbulent flow and low substrate concentration. Bioprocess Engineering, 20(4), 363-368.

Annexure

TABLE A1: Calibration data of rotameter.

Flow rate (LPM)	Flow rate (LPH)	Test-1	Test-2	Test-3	Test-4	Test-5	Test-6	Test-7	Test-8
16	960	968	966	964	965	966	967	963	964
20	1200	1205	1203	1206	1204	1203	1205	1202	1204
24	1440	1443	1444	1442	1445	1441	1442	1446	1445
28	1680	1684	1683	1682	1683	1681	1685	1684	1683
32	1920	1930	1925	1922	1924	1926	1928	1925	1924
36	2160	2165	2164	2163	2164	2162	2166	2165	2164
40	2400	2415	2410	2407	2406	2405	2406	2407	2407

TABLE A2: pH of guar gum and hydroxyethyl cellulose.

S.NO	Concentration (in ppm)	pH (GG)	pH (HEC)
1	3000	4.52	7.87
2	2500	4.75	7.95
3	2000	5.3	8.05
4	1500	6.47	8.13
5	1000	6.7	8.2

TABLE A3: Mechanical degradation of guar gum with 1000 ppm solution at different flow rates.

Time (in minutes)	16 LPM	20 LPM	24 LPM	28 LPM	32 LPM	36 LPM	40 LPM
1	25.40633	35.02994	42.10329	50.81266	53.12233	56.29812	60.00321
2	25.40633	35.02994	42.10329	50.81266	53.12233	56.29812	60.00321
3	25.40633	35.02994	42.10329	50.81266	53.12233	54.54662	57.49145
4	23.81843	32.77802	39.5771	48.69547	50.81266	54.54662	57.49145
5	23.81843	32.77802	39.5771	48.69547	50.81266	52.54491	57.49145
6	23.81843	32.77802	39.5771	48.69547	50.81266	52.54491	54.42151
7	21.17194	29.02481	34.5247	44.46108	45.73139	49.79256	54.42151
8	21.17194	29.02481	34.5247	44.46108	45.73139	49.79256	52.46792
9	21.17194	29.02481	34.5247	44.46108	40.41916	49.79256	52.46792
10	18.52545	27.77374	30.31437	40.22669	40.41916	44.53807	49.03518
11	18.52545	27.77374	30.31437	40.22669	40.41916	44.53807	49.03518
12	18.52545	27.77374	30.31437	40.22669	36.95466	44.53807	49.03518
13	16.40826	24.39585	26.94611	34.29855	36.95466	39.784	46.04897
14	16.40826	24.39585	26.94611	34.29855	34.645	39.784	46.04897

15	16.40826	24.39585	21.89371	34.29855	34.645	34.77973	43.25813
16	13.76176	20.89286	21.89371	30.69932	34.645	34.77973	43.25813
17	13.76176	20.89286	21.89371	30.69932	30.4876	30.27588	41.8627
18	13.76176	20.89286	19.03069	30.69932	30.4876	30.27588	41.8627
19	11.85629	18.76604	19.03069	25.82977	30.4876	25.2716	35.72284
20	11.85629	18.76604	19.03069	25.82977	24.2515	25.2716	35.72284
21	11.85629	18.76604	15.49401	25.82977	24.2515	23.77032	28.46664
22	9.527374	12.6358	15.49401	20.11334	24.2515	23.77032	28.46664
23	9.527374	12.6358	15.49401	20.11334	20.787	21.26818	26.51305
24	9.527374	12.6358	12.12575	17.99615	20.787	21.26818	26.51305
25	7.939478	10.63409	12.12575	17.99615	20.787	19.51668	23.7222
26	7.939478	10.63409	12.12575	15.9213	17.55346	19.51668	23.7222
27	7.939478	8.895103	9.262725	15.9213	17.55346	17.76518	20.93135
28	5.822284	8.895103	9.262725	12.70317	15.70573	17.76518	20.93135
29	5.822284	7.75663	8.504865	12.70317	15.70573	16.2639	18.97776
30	5.822284	7.75663	8.504865	11.00941	13.858	16.2639	18.97776

TABLE A4: Mechanical degradation of guar gum with 1500 ppm solution at different flow rates.

Time (in minutes)	16 LPM	20 LPM	24 LPM	28 LPM	32 LPM	36 LPM	40 LPM
1	28.58212	38.78315	45.47156	53.98845	56.58683	60.55175	64.74765
2	28.58212	38.78315	45.47156	53.98845	56.58683	60.55175	64.74765
3	28.58212	38.78315	45.47156	53.98845	56.58683	59.5509	61.67772
4	26.46493	35.02994	42.94536	51.87126	53.12233	59.5509	61.67772
5	26.46493	35.02994	42.94536	51.87126	53.12233	57.54919	61.67772
6	26.46493	35.02994	42.94536	51.87126	53.12233	57.54919	58.60778
7	24.87703	32.77802	37.89296	47.63687	48.50299	54.54662	58.60778
8	24.87703	32.77802	37.89296	47.63687	48.50299	54.54662	56.09602
9	24.87703	32.77802	37.89296	47.63687	45.03849	54.54662	56.09602
10	21.17194	30.6512	33.68264	43.40248	45.03849	49.54234	53.58426
11	21.17194	30.6512	33.68264	43.40248	45.03849	49.54234	53.58426
12	21.17194	30.6512	33.68264	43.40248	41.574	49.54234	53.58426
13	18.52545	26.89799	28.96707	37.89778	41.574	44.28785	50.23524
14	18.52545	26.89799	28.96707	37.89778	39.26433	44.28785	50.23524
15	18.52545	26.89799	23.57784	37.89778	39.26433	39.53379	47.4444
16	14.60864	22.51925	23.57784	33.87511	39.26433	39.53379	47.4444
17	14.60864	22.51925	23.57784	33.87511	35.79983	35.28015	45.21172
18	14.60864	22.51925	20.20958	33.87511	35.79983	35.28015	45.21172
19	12.91488	20.64264	20.20958	28.58212	35.79983	30.27588	39.07186
20	12.91488	20.64264	20.20958	28.58212	28.87083	30.27588	39.07186
21	12.91488	20.64264	16.84132	28.58212	28.87083	28.77459	32.09474
22	10.59656	13.76176	16.84132	23.28914	28.87083	28.77459	32.09474
23	10.59656	13.76176	16.84132	23.28914	24.13601	25.02139	30.9784

24	10.59656	13.76176	13.47305	20.11334	24.13601	25.02139	30.9784
25	8.468777	11.25962	13.47305	20.11334	24.13601	23.77032	27.90847
26	8.468777	11.25962	13.47305	18.84303	21.94183	23.77032	27.90847
27	8.468777	8.757485	10.44162	18.84303	21.94183	21.26818	24.55945
28	6.986741	8.757485	10.44162	15.87896	19.63216	21.26818	24.55945
29	6.986741	7.75663	9.262725	15.87896	19.63216	20.51754	22.88494
30	6.986741	7.75663	9.262725	13.76176	17.3225	20.51754	22.88494

TABLE A5: Mechanical degradation of guar gum with 2000 ppm solution at different flow rates.

Time (in minutes)	16 LPM	20 LPM	24 LPM	28 LPM	32 LPM	36 LPM	40 LPM
1	31.75791	43.78743	53.89222	59.28144	62.36099	66.55689	69.77117
2	31.75791	43.78743	50.52395	59.28144	62.36099	66.55689	69.77117
3	31.75791	43.78743	50.52395	59.28144	62.36099	64.55518	66.98033
4	28.58212	40.03422	47.15569	57.16424	58.89649	64.55518	66.98033
5	28.58212	40.03422	47.15569	57.16424	58.89649	62.55347	66.98033
6	28.58212	40.03422	47.15569	57.16424	58.89649	62.55347	63.63131
7	25.40633	37.53208	42.10329	52.92986	53.12233	59.5509	63.63131
8	25.40633	37.53208	42.10329	52.92986	53.12233	59.5509	61.39863
9	25.40633	37.53208	42.10329	52.92986	49.65783	59.5509	61.39863
10	22.23054	35.02994	38.73503	48.69547	49.65783	54.54662	58.60778
11	22.23054	35.02994	38.73503	48.69547	49.65783	54.54662	58.60778
12	22.23054	35.02994	38.73503	48.69547	45.03849	54.54662	58.60778
13	19.05475	31.27673	33.68264	42.34388	45.03849	49.54234	55.81694
14	19.05475	31.27673	33.68264	42.34388	43.88366	49.54234	55.81694
15	19.05475	31.27673	28.63024	42.34388	43.88366	44.91339	52.46792
16	15.87896	27.52352	28.63024	38.1095	43.88366	44.91339	52.46792
17	15.87896	27.52352	28.63024	38.1095	39.26433	39.53379	50.23524
18	15.87896	27.52352	25.26198	38.1095	39.26433	39.53379	50.23524
19	13.76176	25.02139	25.26198	33.87511	39.26433	34.90483	44.65355
20	13.76176	25.02139	25.26198	33.87511	32.33533	34.90483	44.65355
21	13.76176	25.02139	21.89371	33.87511	32.33533	32.5278	37.67643
22	11.64457	18.76604	21.89371	27.52352	32.33533	32.5278	37.67643
23	11.64457	18.76604	18.52545	27.52352	26.56116	29.52524	35.72284
24	11.64457	18.76604	18.52545	23.28914	26.56116	29.52524	35.72284
25	9.527374	15.01283	18.52545	23.28914	26.56116	27.52352	32.09474
26	9.527374	15.01283	15.15719	21.17194	24.2515	27.52352	32.09474
27	9.527374	11.25962	15.15719	21.17194	24.2515	25.02139	29.30389
28	7.41018	11.25962	15.15719	16.93755	21.94183	25.02139	29.30389
29	7.41018	8.757485	11.78892	16.93755	21.94183	23.5201	27.90847
30	7.41018	8.757485	11.78892	14.82036	18.47733	23.5201	27.90847

TABLE A6: Mechanical degradation of guar gum with 2500 ppm solution at different flow rates.

Time (in minutes)	16 LPM	20 LPM	24 LPM	28 LPM	32 LPM	36 LPM	40 LPM
1	37.0509	46.28956	53.89222	63.51583	66.98033	70.05988	72.56202
2	37.0509	46.28956	53.89222	63.51583	66.98033	70.05988	72.56202
3	37.0509	46.28956	53.89222	63.51583	66.98033	67.55774	69.77117
4	34.9337	43.78743	50.52395	59.28144	62.36099	67.55774	69.77117
5	34.9337	43.78743	50.52395	59.28144	62.36099	65.0556	69.77117
6	34.9337	43.78743	50.52395	59.28144	62.36099	65.0556	66.98033
7	34.9337	40.03422	45.47156	55.04705	57.74166	62.55347	66.98033
8	31.75791	40.03422	45.47156	55.04705	57.74166	62.55347	64.18948
9	31.75791	36.28101	45.47156	55.04705	53.12233	62.55347	64.18948
10	31.75791	36.28101	42.10329	50.81266	53.12233	57.54919	61.39863
11	28.58212	36.28101	42.10329	50.81266	53.12233	57.54919	61.39863
12	28.58212	31.27673	42.10329	50.81266	48.50299	57.54919	61.39863
13	23.28914	31.27673	38.73503	46.57827	48.50299	52.54491	58.60778
14	23.28914	31.27673	38.73503	46.57827	46.19333	52.54491	58.60778
15	23.28914	27.52352	38.73503	46.57827	46.19333	47.54063	55.81694
16	21.17194	27.52352	33.68264	42.34388	46.19333	47.54063	55.81694
17	21.17194	27.52352	33.68264	42.34388	41.574	42.53636	53.02609
18	21.17194	23.77032	28.63024	42.34388	41.574	42.53636	53.02609
19	19.05475	23.77032	28.63024	38.1095	41.574	37.53208	47.4444
20	19.05475	23.77032	28.63024	38.1095	34.645	37.53208	47.4444
21	15.87896	20.01711	23.57784	38.1095	34.645	35.02994	41.8627
22	15.87896	20.01711	23.57784	31.75791	34.645	35.02994	41.8627
23	13.76176	20.01711	23.57784	31.75791	27.716	32.5278	39.07186
24	13.76176	16.2639	20.20958	25.40633	27.716	32.5278	39.07186
25	13.23246	16.2639	20.20958	25.40633	27.716	30.02566	36.28101
26	13.23246	16.2639	20.20958	21.17194	25.40633	30.02566	36.28101
27	12.70317	12.51069	16.84132	21.17194	25.40633	27.52352	33.49016
28	12.70317	12.51069	16.84132	19.05475	23.09666	27.52352	33.49016
29	8.468777	12.51069	16.84132	19.05475	23.09666	27.52352	30.69932
30	8.468777	10.00855	13.47305	16.93755	20.787	25.02139	30.69932

TABLE A7: Mechanical degradation of guar gum with 3000 ppm solution at different flow rates.

Time (in minutes)	16 LPM	20 LPM	24 LPM	28 LPM	32 LPM	36 LPM	40 LPM
1	42.34388	50.04277	58.94461	67.75021	71.59966	72.56202	75.35287
2	42.34388	50.04277	58.94461	67.75021	71.59966	72.56202	75.35287
3	42.34388	50.04277	58.94461	67.75021	71.59966	70.05988	72.56202
4	39.16809	46.28956	55.57635	63.51583	66.98033	70.05988	72.56202
5	39.16809	46.28956	55.57635	63.51583	66.98033	67.55774	72.56202
6	37.0509	46.28956	55.57635	63.51583	66.98033	67.55774	69.77117
7	37.0509	43.78743	55.57635	63.51583	60.05133	62.55347	69.77117
8	33.87511	43.78743	50.52395	57.16424	60.05133	62.55347	66.98033
9	33.87511	43.78743	50.52395	57.16424	57.74166	62.55347	66.98033
10	31.75791	40.03422	50.52395	57.16424	57.74166	55.04705	64.18948
11	31.75791	40.03422	50.52395	57.16424	55.43199	55.04705	64.18948
12	28.58212	40.03422	45.47156	52.92986	55.43199	55.04705	64.18948
13	28.58212	37.53208	45.47156	52.92986	50.81266	52.54491	61.39863
14	26.46493	37.53208	45.47156	52.92986	50.81266	52.54491	61.39863
15	26.46493	37.53208	42.10329	52.92986	46.19333	50.04277	58.60778
16	26.46493	31.27673	42.10329	46.57827	46.19333	50.04277	58.60778
17	24.34773	31.27673	42.10329	46.57827	46.19333	47.54063	55.81694
18	24.34773	31.27673	37.0509	46.57827	39.26433	47.54063	55.81694
19	21.17194	27.52352	37.0509	46.57827	39.26433	45.03849	53.02609
20	21.17194	27.52352	37.0509	40.22669	39.26433	45.03849	53.02609
21	21.17194	25.02139	31.9985	40.22669	34.645	40.03422	44.65355
22	17.99615	25.02139	31.9985	40.22669	34.645	40.03422	44.65355
23	17.99615	25.02139	31.9985	31.75791	34.645	35.02994	41.8627
24	15.87896	21.26818	26.94611	31.75791	30.02566	35.02994	41.8627
25	15.87896	21.26818	26.94611	31.75791	30.02566	32.5278	39.07186
26	15.87896	18.76604	26.94611	25.40633	27.716	32.5278	39.07186
27	12.70317	18.76604	21.89371	25.40633	27.716	30.02566	36.28101
28	12.70317	15.01283	21.89371	25.40633	25.40633	30.02566	36.28101
29	10.58597	15.01283	21.89371	19.05475	25.40633	27.52352	33.49016
30	10.58597	12.51069	16.84132	19.05475	23.09666	27.52352	33.49016

TABLE A8: Mechanical degradation of hydroxyethyl cellulose with 1000 ppm solution at different flow rates.

Time (in minutes)	16 LPM	20 LPM	24 LPM	28 LPM	32 LPM	36 LPM	40 LPM
1	32.81651	40.03422	47.3241	56.10565	60.05133	63.05389	65.5849
2	32.81651	40.03422	47.3241	56.10565	60.05133	63.05389	65.5849
3	32.81651	40.03422	47.3241	56.10565	60.05133	61.3024	63.63131

4	30.69932	37.53208	44.12425	54.62361	57.27973	61.3024	63.63131
5	30.69932	37.53208	44.12425	54.62361	57.27973	59.80111	63.63131
6	30.69932	37.53208	44.12425	54.62361	57.27973	59.80111	60.00321
7	28.68798	34.40441	40.41916	50.81266	52.66039	56.29812	60.00321
8	28.68798	34.40441	40.41916	50.81266	52.66039	56.29812	58.3287
9	28.68798	34.40441	40.41916	50.81266	47.34816	56.29812	58.3287
10	25.93563	32.77802	36.20883	46.78999	47.34816	52.79512	55.25877
11	25.93563	32.77802	36.20883	46.78999	47.34816	52.79512	55.25877
12	25.93563	32.77802	36.20883	46.78999	44.34559	52.79512	55.25877
13	23.50086	30.6512	33.51422	40.22669	44.34559	47.54063	52.74701
14	23.50086	30.6512	33.51422	40.22669	42.03593	47.54063	52.74701
15	23.50086	30.6512	28.63024	40.22669	42.03593	42.53636	49.11891
16	20.11334	27.39842	28.63024	36.41574	42.03593	42.53636	49.11891
17	20.11334	27.39842	28.63024	36.41574	38.1095	38.03251	47.4444
18	20.11334	27.39842	26.94611	36.41574	38.1095	38.03251	47.4444
19	18.52545	25.2716	26.94611	31.75791	38.1095	33.77887	42.42087
20	18.52545	25.2716	26.94611	31.75791	32.79726	33.77887	42.42087
21	18.52545	25.2716	22.23054	31.75791	32.79726	31.27673	35.72284
22	16.93755	20.26732	22.23054	27.10009	32.79726	31.27673	35.72284
23	16.93755	20.26732	22.23054	27.10009	28.17793	29.52524	33.43435
24	16.93755	20.26732	20.20958	24.13601	28.17793	29.52524	33.43435
25	14.82036	18.76604	20.20958	24.13601	28.17793	27.27331	30.69932
26	14.82036	18.76604	20.20958	22.8657	26.56116	27.27331	30.69932
27	14.82036	16.51411	18.02021	22.8657	26.56116	25.02139	27.3503
28	12.70317	16.51411	18.02021	19.47819	24.2515	25.02139	27.3503
29	12.70317	15.26305	16.84132	19.47819	24.2515	24.02053	25.67579
30	12.70317	15.26305	16.84132	18.8642	22.63473	24.02053	25.67579

TABLE A9: Mechanical degradation of hydroxyethyl cellulose with 1500 ppm solution at different flow rates.

Time (in minutes)	16 LPM	20 LPM	24 LPM	28 LPM	32 LPM	36 LPM	40 LPM
1	35.9923	43.78743	51.02919	58.22284	62.36099	65.0556	67.25941
2	35.9923	43.78743	51.02919	58.22284	62.36099	65.0556	67.25941
3	35.9923	43.78743	51.02919	58.22284	62.36099	63.05389	64.74765
4	33.98097	40.65975	48.83982	56.7408	59.82036	63.05389	64.74765
5	33.98097	40.65975	48.83982	56.7408	59.82036	61.3024	64.74765
6	33.98097	40.65975	48.83982	56.7408	59.82036	61.3024	61.67772
7	31.75791	37.53208	43.95584	52.50642	54.97006	58.04962	61.67772
8	31.75791	37.53208	43.95584	52.50642	54.97006	58.04962	59.16595
9	31.75791	37.53208	43.95584	52.50642	51.96749	58.04962	59.16595
10	28.79384	35.28015	39.07186	48.48375	51.96749	53.04534	57.21236

11	28.79384	35.28015	39.07186	48.48375	51.96749	53.04534	57.21236
12	28.79384	35.28015	39.07186	48.48375	47.34816	53.04534	57.21236
13	25.61805	32.77802	35.36677	43.40248	47.34816	48.7917	54.42151
14	25.61805	32.77802	35.36677	43.40248	45.03849	48.7917	54.42151
15	25.61805	32.77802	33.51422	43.40248	45.03849	43.78743	51.63067
16	22.23054	28.77459	33.51422	39.37981	45.03849	43.78743	51.63067
17	22.23054	28.77459	33.51422	39.37981	41.34303	39.53379	49.67707
18	22.23054	28.77459	30.6512	39.37981	41.34303	39.53379	49.67707
19	20.64264	26.52267	30.6512	34.29855	41.34303	34.52951	43.8163
20	20.64264	26.52267	30.6512	34.29855	36.49273	34.52951	43.8163
21	20.64264	26.52267	26.77769	34.29855	36.49273	34.52951	37.67643
22	18.52545	22.76946	26.77769	29.21728	36.49273	32.27759	37.67643
23	18.52545	22.76946	26.77769	29.21728	32.33533	32.27759	35.16467
24	18.52545	22.76946	23.91467	26.46493	32.33533	29.52524	35.16467
25	16.72583	20.01711	23.91467	26.46493	32.33533	29.52524	32.65291
26	16.72583	20.01711	23.91467	24.55945	28.17793	27.52352	32.65291
27	16.72583	18.64093	20.20958	24.55945	28.17793	27.52352	29.30389
28	14.82036	18.64093	20.20958	22.23054	25.6373	25.02139	29.30389
29	14.82036	16.88944	18.86228	22.23054	25.6373	25.02139	27.3503
30	14.82036	16.88944	18.86228	20.32506	23.5586	25.02139	27.3503

TABLE A10: Mechanical degradation of hydroxyethyl cellulose with 2000 ppm solution at different flow rates.

Time (in minutes)	16 LPM	20 LPM	24 LPM	28 LPM	32 LPM	36 LPM	40 LPM
1	38.1095	46.28956	55.57635	61.39863	64.90163	68.5586	71.1666
2	38.1095	46.28956	55.57635	61.39863	64.90163	68.5586	71.1666
3	38.1095	46.28956	55.57635	61.39863	64.90163	66.30667	69.49209
4	35.9923	44.41296	52.54491	59.28144	61.20616	66.30667	69.49209
5	35.9923	44.41296	52.54491	59.28144	61.20616	64.55518	69.49209
6	35.9923	44.41296	52.54491	59.28144	61.20616	64.55518	66.42216
7	32.92237	41.5355	47.49252	55.25877	56.58683	61.3024	66.42216
8	32.92237	41.5355	47.49252	55.25877	56.58683	61.3024	64.74765
9	32.92237	41.5355	47.49252	55.25877	53.35329	61.3024	64.74765
10	29.64072	39.28358	43.78743	51.2361	53.35329	56.79855	61.11955
11	29.64072	39.28358	43.78743	51.2361	53.35329	56.79855	61.11955
12	29.64072	39.28358	43.78743	51.2361	50.81497	56.79855	61.11955
13	26.57079	35.28015	38.3982	46.15483	50.81497	51.54406	58.88687
14	26.57079	35.28015	38.3982	46.15483	48.50299	51.54406	58.88687
15	26.57079	35.28015	34.5247	46.15483	48.50299	49.54234	56.37511
16	22.75984	31.52695	34.5247	42.34388	48.50299	49.54234	56.37511
17	22.75984	31.52695	34.5247	42.34388	44.80753	45.53892	54.7006

18	22.75984	31.52695	32.33533	42.34388	44.80753	45.53892	54.7006
19	20.11334	29.40013	32.33533	38.53293	44.80753	40.28443	48.83982
20	20.11334	29.40013	32.33533	38.53293	37.00086	40.28443	48.83982
21	20.11334	29.40013	28.96707	38.53293	37.00086	38.03251	41.58362
22	18.74775	23.14478	28.96707	32.81651	37.00086	38.03251	41.58362
23	18.74775	23.14478	26.94611	32.81651	31.1805	35.53037	39.63003
24	18.74775	23.14478	26.94611	28.58212	31.1805	35.53037	39.63003
25	16.93755	20.64264	26.94611	28.58212	31.1805	33.77887	36.83918
26	16.93755	20.64264	21.89371	28.58212	29.56373	33.77887	36.83918
27	16.93755	18.89115	21.89371	26.25321	29.56373	31.27673	33.76925
28	14.92622	18.89115	21.89371	26.25321	28.20334	31.27673	33.76925
29	14.92622	16.88944	19.36752	22.23054	28.20334	29.52524	31.00631
30	14.92622	16.88944	19.36752	22.23054	25.66039	29.52524	31.00631

TABLE A11: Mechanical degradation of hydroxyethyl cellulose with 2500 ppm solution at different flow rates.

Time (in minutes)	16 LPM	20 LPM	24 LPM	28 LPM	32 LPM	36 LPM	40 LPM
1	43.40248	51.41895	58.10255	65.63302	68.82806	72.56202	74.23653
2	43.40248	51.41895	58.10255	65.63302	68.82806	72.56202	74.23653
3	43.40248	51.41895	58.10255	65.63302	68.82806	69.80967	71.1666
4	40.43841	48.7917	55.57635	61.39863	64.67066	69.80967	71.1666
5	40.43841	48.7917	55.57635	61.39863	64.67066	67.55774	71.1666
6	40.43841	48.7917	55.57635	61.39863	64.67066	67.55774	68.37575
7	40.43841	45.03849	50.52395	57.58768	60.05133	64.80539	68.37575
8	37.15676	45.03849	50.52395	57.58768	60.05133	64.80539	66.42216
9	37.15676	41.41039	50.52395	57.58768	56.58683	64.80539	66.42216
10	37.15676	41.41039	47.49252	52.92986	56.58683	59.5509	63.91039
11	34.08683	41.41039	47.49252	52.92986	56.58683	59.5509	63.91039
12	34.08683	36.28101	47.49252	52.92986	51.27459	59.5509	63.91039
13	29.21728	36.28101	43.78743	48.69547	51.27459	54.54662	60.00321
14	29.21728	36.28101	43.78743	48.69547	49.19589	54.54662	60.00321
15	29.21728	32.77802	43.78743	48.69547	49.19589	49.79256	57.21236
16	27.52352	32.77802	38.73503	44.03764	49.19589	49.79256	57.21236
17	27.52352	32.77802	38.73503	44.03764	44.34559	45.28871	55.95648
18	27.52352	29.40013	33.85105	44.03764	44.34559	45.28871	55.95648
19	25.82977	29.40013	33.85105	40.22669	44.34559	40.28443	49.67707
20	25.82977	29.40013	33.85105	40.22669	38.36356	40.28443	49.67707
21	21.70124	26.27246	28.96707	40.22669	38.36356	38.78315	43.53721
22	21.70124	26.27246	28.96707	35.9923	38.36356	38.78315	43.53721
23	19.90163	26.27246	28.96707	35.9923	33.49016	34.52951	41.30453
24	19.90163	23.64521	25.5988	32.81651	33.49016	34.52951	41.30453

25	19.90163	23.64521	25.5988	32.81651	33.49016	33.77887	38.51369
26	19.90163	23.64521	25.5988	32.81651	30.02566	33.77887	38.51369
27	18.10201	21.26818	23.24102	28.58212	30.02566	32.5278	35.72284
28	18.10201	21.26818	23.24102	28.58212	30.02566	32.5278	35.72284
29	14.82036	16.2639	23.24102	25.40633	28.87083	32.5278	32.93199
30	14.82036	16.2639	19.36752	25.40633	28.87083	30.52609	32.93199

TABLE A12: Mechanical degradation of hydroxyethyl cellulose with 3000 ppm solution at different flow rates.

Time (in minutes)	16 LPM	20 LPM	24 LPM	28 LPM	32 LPM	36 LPM	40 LPM
1	47.63687	56.29812	65.68114	69.86741	73.90932	75.06416	77.58554
2	47.63687	56.29812	65.68114	69.86741	73.90932	75.06416	77.58554
3	47.63687	56.29812	65.68114	69.86741	73.90932	73.56287	75.35287
4	44.46108	52.54491	60.62874	65.84474	69.28999	73.56287	75.35287
5	44.46108	52.54491	60.62874	65.84474	69.28999	70.05988	75.35287
6	44.46108	52.54491	60.62874	65.84474	69.28999	70.05988	72.56202
7	40.22669	50.04277	57.26048	65.84474	64.67066	65.0556	72.56202
8	40.22669	50.04277	57.26048	59.28144	64.67066	65.0556	69.77117
9	40.22669	50.04277	57.26048	59.28144	60.05133	65.0556	69.77117
10	37.0509	46.28956	50.52395	59.28144	60.05133	62.80368	66.98033
11	37.0509	46.28956	50.52395	59.28144	58.20359	62.80368	64.18948
12	37.0509	46.28956	50.52395	54.62361	58.20359	62.80368	64.18948
13	33.87511	43.78743	45.47156	54.62361	53.12233	58.80026	61.39863
14	33.87511	43.78743	45.47156	54.62361	53.12233	58.80026	61.39863
15	33.87511	43.78743	45.47156	54.62361	49.65783	53.79598	59.86367
16	28.58212	38.78315	42.10329	48.69547	49.65783	53.79598	59.86367
17	28.58212	38.78315	42.10329	48.69547	49.65783	50.5432	57.21236
18	28.58212	38.78315	42.10329	48.69547	42.72883	50.5432	57.21236
19	26.46493	35.02994	37.0509	48.69547	42.72883	48.7917	55.81694
20	26.46493	35.02994	37.0509	42.34388	42.72883	48.7917	55.81694
21	26.46493	35.02994	37.0509	42.34388	38.1095	43.78743	46.88623
22	23.28914	31.27673	33.68264	42.34388	38.1095	43.78743	46.88623
23	23.28914	31.27673	33.68264	35.9923	38.1095	38.78315	43.25813
24	23.28914	31.27673	33.68264	35.9923	34.645	38.78315	43.25813
25	21.17194	27.52352	30.31437	35.9923	34.645	38.78315	41.8627
26	21.17194	27.52352	30.31437	33.87511	32.33533	36.0308	41.8627
27	21.17194	25.02139	26.94611	33.87511	32.33533	36.0308	38.51369
28	16.93755	25.02139	26.94611	33.87511	32.33533	32.5278	38.51369
29	16.93755	20.01711	26.94611	28.58212	27.716	32.5278	36.28101
30	12.70317	20.01711	21.89371	28.58212	27.716	27.52352	36.28101